On the Accuracy Limits of Misspecified Delay-Doppler Estimation

Article *in* Signal Processing · November 2022

DOI: 10.1016/j.sigpro.2022.108872

4 authors:

Hamish McPhee
Telecommunications for Space and Aeronautics

Lorenzo Ortega Espluga
Institut Polytechnique des Sciences Avancées

Jordi Vilà-Valls
Institut Supérieur de l'Aéronautique et de l'Espace (ISAE)

E. Chaumette
Institut Supérieur de l'Aéronautique et de l'Espace (ISAE)

On the Accuracy Limits of Misspecified Delay-Doppler Estimation

Hamish McPhee[a,*], Lorenzo Ortega[a,b], Jordi Vilà-Valls[c], Eric Chaumette[c]

[a] *TéSA, Toulouse, France.*
[b] *IPSA, Toulouse, France.*
[c] *ISAE-SUPAERO/University of Toulouse, Toulouse, France.*

Abstract

This work derives compact closed-form expressions of the misspecified Cramér-Rao bound and pseudo-true parameters of time-delay and Doppler for a high dynamics signal model. Those expressions are validated by analyzing the mean square error (MSE) of the misspecified maximum likelihood estimator. A noteworthy outcome of these MSE results is that, for some magnitudes of acceleration and signal-to-noise ratios, neglecting the acceleration is beneficial in the MSE sense. The variance performance improvement is obtained at the cost of a systematic error in the true parameter estimation. This can be seen as a specific case of the trade-off between bias and variance. Neglecting the acceleration can improve the Doppler estimation when the error induced on the misspecified model is less than the variance increase due to including an extra parameter to estimate. Then, for some non-zero acceleration magnitudes and short integration times, the Doppler estimation using a misspecified model outperforms a correctly specified model in the MSE sense.

Keywords: Misspecified maximum likelihood estimator, time-delay, Doppler, acceleration, misspecified Cramér-Rao bound

1. Introduction

The estimation of deterministic signal parameters is a key component for several applications such as Global Navigation Satellite Systems (GNSS) [1], radar or sonar [2]. In these types of applications, a main objective is to identify several parameters of interest from a noisy signal observation. This problem has received considerable attention during the last fifty years, both for time-series analysis [3] and array processing [4], and merged into the framework of modern array processing [5, 4]. The noisy signal observation can usually be modeled through a parameterised distribution model, e.g., a Complex-Gaussian distribution with some mean and variance. In certain circumstances, the parameterised distribution model can be deliberately misspecified to simplify the estimation of the parameters of interest [6, 7]. A possible misspecification involves choosing fewer parameters to estimate than the ones that truly influence the signal dynamics. For

*Corresponding author
Email address: hamish.mcphee@tesa.prd.fr (Hamish McPhee)

example, a common assumption in the above mentioned applications is that the effects due to the acceleration of the receiver and/or target are negligible. In other words, instead of using a receiver structure that attempts to perform the joint estimation of the time-delay, Doppler and acceleration, only a joint estimation of the time-delay and Doppler is performed. Note that there are certain articles in the state-of-the-art where Cramér-Rao bounds (CRBs) were developed for sparse parameters estimation, where some of the estimated parameters are set to zero to account for missing observations [8, 9]. In this contribution, we neglect the acceleration as a method of reducing the estimation demand in the case we still have full observations. Our work differs from the sparse estimation bounds because we have the ability to estimate acceleration and choose not to, as opposed to sparse estimation being a case where certain parameters cannot be estimated.

In general, a reduced number of estimated parameters for the same amount of observations will decrease the demand of the estimator and allow an improvement in variance. The exclusion of acceleration in the statistical model means that the joint estimation of time-delay and Doppler is misspecified. As a consequence, the estimates will have a systematic error introduced due to not accounting for the acceleration effects on the other parameters. We can define a high dynamics scenario as the case where the acceleration magnitude is sufficient enough that this systematic error is noticeable. The systematic error is represented by the difference between the expected value of the misspecified estimates and their respective true values.

Compact closed-form expressions of the CRB for parameterised receiver architectures have been presented for the GNSS and radar systems in [10] for time-delay and Doppler, and in [11] for time-delay, Doppler and acceleration, when considering a band-limited signal. In these articles, the performance limits in a mean square error (MSE) sense were validated thanks to the maximum likelihood estimator (MLE), which is known to be asymptotically efficient [12]. However, the specific MSE performance limits when considering a misspecified receiver architecture [13], i.e., neglecting a non-zero acceleration, have not yet been presented. The misspecified MLE (MMLE) performance limit depends on the error induced when considering a misspecified model, as well as the variance of the associated parameter estimation, which is bounded by the misspecified CRB (MCRB) [7, 14, 13, 15, 16]. This article contributes a new compact closed-form expression for the MCRB of the time-delay and Doppler parameters under high dynamics scenarios. Since the closed-form equations depend only on the signal samples, reader's can easily compute the specific delay-Doppler MCRB for any signal model with acceleration present.

The derivation of the MCRB follows from a generalized Slepian-form of two information matrices $\mathbf{A}$ and $\mathbf{B}$, which depend on the so-called pseudo-true parameters [14]. The pseudo-true parameters are the values of the misspecified parameters that minimise the Kullback Leibler Distance (KLD) between the true and misspecified distribution models. The error on the delay and Doppler estimates due to neglecting the acceleration is determined as the deviation of the pseudo-true parameter from the corresponding true value. We analyse the MSE performance of the MMLE with respect to (w.r.t.) both pseudo-true and true parameters. We can verify the derivation of the MCRB by checking that the MSE w.r.t. the pseudo-true parameters converges asymptotically to the MCRB [17, 18]. Finally, we compare the MSE of the MMLE solution with respect to the MSE of the fully specified MLE. A noteworthy outcome of these results is that, for some magnitudes of acceleration and signal-to-noise ratios (SNRs), neglecting the acceleration is beneficial in the MSE sense, that is, the Doppler estimation using a misspecified model outperforms a correctly specified model in the MSE sense, which is a new result of practical importance in several applications.

The article is organized as follows: Section 2 presents the received signal model under high dynamics. Section 3 details the misspecified signal model and the pseudo-true parameters. In Section 4, closed-form expressions of the pseudo-true parameters are derived. In Section 5, a new compact closed-form expression of the MCRB for joint time-delay and Doppler is presented. The theoretical expressions of the bounds are validated and discussed together with MMLE and MLE simulations in Section 6.

Notation

Scalar values are defined in italic (a), vector in bold lower-case ($\mathbf{a}$), and matrices bold upper-case ($\mathbf{A}$). $||\mathbf{x}|| = \sqrt{\sum_{n=1}^{N} x_i^2}$ is the L^2 norm of vector $\mathbf{x}$ with N elements and $|x|$ gives the absolute value of the scalar x. The transpose operation is indicated by the superscript ^{T}, the conjugate transpose by the superscript ^{H}, and the conjugate operation by the superscript *. $\mathbf{I}_N$ represents the identity matrix of dimension N, $\mathrm{Re}\{\cdot\}$ and $\mathrm{Im}\{\cdot\}$ refer to the real part and the imaginary part.

2. Signal Model

The signal model must be defined to appropriately present the true and the misspecified parameterizations used at the receiver. For this work, we consider the line-of-sight (LOS) transmission of a single band-limited signal $s(t)$ with sampling frequency f_s over a carrier with frequency f_c (wavelength $\lambda_c = c/f_c$). The signal travels from a transmitter at position $\mathbf{p}_T(t)$ to a receiver at position $\mathbf{p}_R(t)$, the signal is expressed in both time and frequency as,

$$s(t) = \sum_{k=-N_1'}^{N_2'} s\left(\frac{k}{f_s}\right) \mathrm{sinc}\left(\pi f_s \left(t - \frac{k}{f_s}\right)\right) \rightleftharpoons S(f) = \frac{1}{f_s} \sum_{k=-N_1'}^{N_2'} s\left(\frac{k}{f_s}\right) e^{-j2\pi k \frac{f}{f_s}}, \ \frac{-f_s}{2} \leq f \leq \frac{f_s}{2}, \tag{1a}$$

where $\rightleftharpoons$ refers to the Fourier transform to the frequency f domain, and $N_1', N_2' \in \mathbb{Z}$. As these values approach infinity the equations give an exact representation of the analog signal in a discretized formulation.

The radial displacement between transmitter and receiver is proportional to the signal time-delay, which is in-turn affected by the relative motion between both transmitter and receiver (i.e., Doppler effect and the relative acceleration if we assume high dynamics scenarios). Thus, the radial displacement between transmitter and receiver $p_{TR}(t) = \|\mathbf{p}_T(t) - \mathbf{p}_R(t)\|$ changes over time depending on the relative velocity $\mathbf{v} = \mathbf{v}_T - \mathbf{v}_R$ and relative acceleration $\mathbf{a} = \mathbf{a}_T - \mathbf{a}_R$ (where $\mathbf{p}_T(t) = \mathbf{p}_T(0) + \mathbf{v}_T t + \frac{1}{2}\mathbf{a}_T t^2$ and $\mathbf{p}_R(t) = \mathbf{p}_R(0) + \mathbf{v}_R t + \frac{1}{2}\mathbf{a}_R t^2$). This distance is used in the ranging equation for tracking of the target $p_{TR}(t; \boldsymbol{\eta}) = c\tau_{true}(t; \boldsymbol{\eta})$, where c is the speed of light and $\tau_{true}(t;\boldsymbol{\eta})$ represents the delay as a function of time and the parameters that impact the perceived signal. Including the acceleration effect expands upon the typically simplified model by allowing estimation of the rate of change of velocity, i.e., Doppler rate. The equation which describes the LOS distance travelled by the transmitted signal is

$$p_{TR}(t;\boldsymbol{\eta}) = \|\mathbf{p}_T\left(t-\tau_{true}(t;\boldsymbol{\eta})\right)-\mathbf{p}_R\left(t\right)\| = c\tau_{true}(t;\boldsymbol{\eta}) \simeq \left\|\mathbf{p}_T(0)-\mathbf{p}_R(0)-\mathbf{v}_{rad}t-\frac{1}{2}\mathbf{a}_{rad}t^2\right\|, \tag{2}$$

since the radial components $\mathbf{v}_{rad}$ and $\mathbf{a}_{rad}$ of the relative velocity and acceleration are the only contributors to change in LOS distance. Therefore, $\tau_{true}\left(t;\boldsymbol{\eta}\right) \simeq \tau + bt + dt^2, \tau = \frac{\|\mathbf{p}_T(0)-\mathbf{p}_R(0)\|}{c}, b = \frac{\|-\mathbf{v}_{rad}\|}{c}, d = \frac{\|-\mathbf{a}_{rad}\|}{2c}$. The complex analytic signal at the antenna output is then a function of the actual delay and modulated by the carrier wave, which is also shifted through multiplication with the Doppler and acceleration parameters,

$$x_A(t) = \alpha_A e^{j2\pi f_c(t-\tau_{true}(t;\boldsymbol{\eta}))} s\left(t-\tau_{true}(t;\boldsymbol{\eta})\right) + n_A(t), \tag{3}$$

with $n_A(t)$ a zero-mean white complex circular Gaussian noise, α_A an amplitude factor that depends on signal power, polarisation vectors and antenna gains [19, 20], and $\boldsymbol{\eta} = [\tau, b, d]^T$ the fully specified parameters, which are considered to appropriately represent the true parameterization of the estimation problem.

The complex analytical signal model is considered to be narrowband ($f_c >> f_s \geq B$, where B is the baseband signal bandwidth and f_s is the Hilbert filter bandwidth), resulting in negligible influence of the Doppler parameter on the signal samples, $s(t-\tau_{true}(t;\boldsymbol{\eta})) \simeq s(t-\tau)$. Hence, for short observation times, a good approximation of the baseband output of the fully specified receiver's Hilbert filter [10], is [21],

$$x\left(t;\boldsymbol{\epsilon}\right) = x_A\left(t\right)e^{-j2\pi f_c t} = \alpha\boldsymbol{\mu}(t;\boldsymbol{\eta}) + n\left(t\right), \tag{4}$$

$$\mu(t;\boldsymbol{\eta}) = s\left(t-\tau\right)e^{-j2\pi f_c(b(t-\tau)+d(t-\tau)^2)}, \tag{5}$$

with $n(t)$ a complex white Gaussian noise within f_s with unknown variance σ_n^2 and $\alpha = \alpha_A e^{-j2\pi f_c\tau(1+b+d\tau)}$ where $\alpha_A = \rho_A e^{j\Phi_A}$, containing the complex amplitude and phase. The discrete vector signal model is built from $N = N_1 + N_2 + 1$ ($N_1/f_s \gg N_1'/B$, $N_2/f_s \gg N_2'B$) samples at $T_s = 1/f_s$,

$$\mathbf{x} = \alpha\boldsymbol{\mu}(\boldsymbol{\eta}) + \mathbf{n} = \rho e^{j\Phi}\boldsymbol{\mu}(\boldsymbol{\eta}) + \mathbf{n}, \tag{6}$$

$$\mathbf{x} = \left(\ldots, x\left(kT_s\right), \ldots\right)^\top,$$

$$\mathbf{n} = \left(\ldots, n\left(kT_s\right), \ldots\right)^\top,$$

$$\boldsymbol{\mu}(\boldsymbol{\eta}) = \left(\ldots, s(kT_s-\tau)e^{-j2\pi f_c(b(kT_s-\tau)+d(kT_s-\tau)^2)}, \ldots\right)^\top,$$

with $-N_1 \leq k \leq N_2$ signal samples. The unknown deterministic parameters can be gathered in vector $\boldsymbol{\epsilon} = \left[\sigma_n^2, \rho, \Phi, \tau, b, d\right]^\top = \left[\sigma_n^2, \rho, \Phi, \boldsymbol{\eta}^\top\right]^\top$, with $\alpha = \rho e^{j\Phi}, \rho \in \mathbb{R}^+, 0 \leq \Phi \leq 2\pi$. We underline that the CRBs associated to the parameters of interest $\boldsymbol{\eta}$ were derived for this particular signal model in [11]. In the sequel we focus on developing the theoretical framework which allows to describe what happens in the case of using a less complex receiver structure, which considers a misspecified signal model. In other words, the receiver structure assumes only that the time-delay and Doppler effects impact the signal propagation delay.

3. Theoretical Framework of a Misspecified Signal Model

The signal model parameterised by delay, Doppler, and acceleration is now referred to as the true model and is the parameterization that would be used by a receiver architecture that considers a fully specified MLE, that is, a matched filter, i.e., a receiver which aims to estimate the parameter of interest $\boldsymbol{\eta} = [\tau, b, d]^T$. The true signal model is represented by a probability density function (pdf) which follows a complex circular Gaussian distribution $\mathbf{x} \sim \mathcal{CN}(\alpha\boldsymbol{\mu}(\boldsymbol{\eta}), \sigma_n^2 \boldsymbol{I}_N)$, with the covariance matrix being a diagonal matrix. On the other hand, the misspecified signal model represents the receiver architecture which does not consider the acceleration parameter, i.e., a MMLE [13] (mismatched filter) is implemented at the receiver. This particular case leads to the definition of the misspecified vector of parameter of interest $\boldsymbol{\omega}' = [\tau', b']^\top$, which is contained in the parameter vector $\boldsymbol{\epsilon}' = \left[\sigma_n^2, \boldsymbol{\theta}'\right]$ with $\boldsymbol{\theta}' = [\rho', \Phi', \boldsymbol{\omega}']$, yielding the following signal model at the output of the Hilbert filter,

$$x(t; \boldsymbol{\epsilon}') = \alpha' s(t - \tau') e^{-j2\pi f_c b'(t-\tau')} + n(t), \tag{7}$$

with $\alpha' = \rho' e^{j\Phi'}$. Again, we can build the discrete vector signal model from $N = N_1 + N_2 + 1$ ($N_1/f_s \gg N_1'/B$, $N_2/f_s \gg N_2' B$) samples at $T_s = 1/f_s$,

$$\mathbf{x}' = \alpha' \mathbf{m}(\boldsymbol{\omega}') + \mathbf{n}, \tag{8}$$

$$\mathbf{m}(\boldsymbol{\omega}') = (\ldots, s(kT_s - \tau') e^{-j2\pi f_c (b'(kT_s - \tau'))}, \ldots)^\top.$$

The misspecified signal model is represented by $\mathbf{x}' \sim \mathcal{CN}(\alpha' \mathbf{m}(\boldsymbol{\omega}'), \sigma_n^2 \boldsymbol{I}_N)$. Note that under this particular scenario, the diagonal covariance matrix of the well specified signal model is the same as the covariance matrix of the misspecified signal model. Moreover, we assume that the covariance matrix does not depend on the parameters of interest, yielding to the following well specified and mispecified pdfs,

$$p(\mathbf{x}; \boldsymbol{\epsilon}) = \frac{1}{\pi^N \sigma_n^{2N}} e^{\frac{-(\mathbf{x} - \alpha\boldsymbol{\mu}(\boldsymbol{\eta}))^H (\mathbf{x} - \alpha\boldsymbol{\mu}(\boldsymbol{\eta}))}{\sigma_n^2}}, \tag{9}$$

$$f(\mathbf{x}; \boldsymbol{\epsilon}') = \frac{1}{\pi^N \sigma_n^{2N}} e^{\frac{-(\mathbf{x} - \alpha'\mathbf{m}(\boldsymbol{\omega}'))^H (\mathbf{x} - \alpha'\mathbf{m}(\boldsymbol{\omega}'))}{\sigma_n^2}}. \tag{10}$$

The estimated parameters of a MMLE are commonly referred to as pseudo-true parameters. We label them with $\boldsymbol{\theta}_{pt} = \left[\rho_{pt}, \Phi_{pt}, \tau_{pt}, b_{pt}\right]$. In the following sections, we will focus on the estimation of these parameters to theoretically calculate the impact on the MSE of the MMLE implementation.

4. Pseudo-True Parameters Computation

The pseudo-true parameters are simply those that give the minimum KLD $D(p_{\boldsymbol{\epsilon}} || f_{\boldsymbol{\epsilon}'})$ between the true and assumed models [22, 13],

$$D(p_{\boldsymbol{\epsilon}} || f_{\boldsymbol{\epsilon}'}) = E_p \left[ln p_{\boldsymbol{\epsilon}}(\mathbf{x}; \boldsymbol{\epsilon}) - ln f_{\boldsymbol{\epsilon}'}(\mathbf{x}; \boldsymbol{\epsilon}') \right], \tag{11}$$

$$\boldsymbol{\theta}_{pt} = \arg\min_{\boldsymbol{\theta}'} \{D(p_{\boldsymbol{\epsilon}}||f_{\boldsymbol{\epsilon}'})\} = \arg\min_{\boldsymbol{\theta}'} \left\{E_p\left[-lnf_{\boldsymbol{\epsilon}'}(\mathbf{x};\boldsymbol{\epsilon}')\right]\right\}, \tag{12}$$

where $E_p[\cdot]$ is the expectation with respect to the true model's pdf. The formula for the KLD is expanded in Appendix A and results in the following function to be minimised.

$$\boldsymbol{\theta}_{pt} = \arg\min_{\boldsymbol{\theta}'} \left\{\|\alpha\boldsymbol{\mu}(\boldsymbol{\eta}) - \alpha'\mathbf{m}(\boldsymbol{\omega}')\|^2\right\} = \arg\min_{\boldsymbol{\theta}'} \left\{\left\|\mathbf{m}(\boldsymbol{\omega}')\left(\alpha\frac{\mathbf{m}(\boldsymbol{\omega}')^H\boldsymbol{\mu}(\boldsymbol{\eta})}{\mathbf{m}(\boldsymbol{\omega}')^H\mathbf{m}(\boldsymbol{\omega}')} - \alpha'\right)\right\|^2 + \left\|\alpha\boldsymbol{\mu}(\boldsymbol{\eta}) - \Pi_{\mathbf{m}(\boldsymbol{\omega}')}\alpha\boldsymbol{\mu}(\boldsymbol{\eta})\right\|^2\right\} \tag{13}$$

The component of the equation that is minimised by α' with $\alpha_{pt} = \rho_{pt}e^{j\Phi_{pt}}$:

$$\Rightarrow \alpha_{pt} = \alpha\frac{\mathbf{m}(\boldsymbol{\omega}_{pt})^H\boldsymbol{\mu}(\boldsymbol{\eta})}{\mathbf{m}(\boldsymbol{\omega}_{pt})^H\mathbf{m}(\boldsymbol{\omega}_{pt})}, \tag{14}$$

and the component that is minimised by $\boldsymbol{\omega}'$, is equivalent to maximising the negative term:

$$\Rightarrow \boldsymbol{\omega}_{pt} = \arg\max_{\boldsymbol{\omega}'} \left\{\left\|\Pi_{\mathbf{m}(\boldsymbol{\omega}')}\alpha\boldsymbol{\mu}(\boldsymbol{\eta})\right\|^2\right\}. \tag{15}$$

These results are effectively the noiseless versions of the MMLE given by [23]

$$\begin{cases} \widehat{\alpha} = \frac{\mathbf{m}(\widehat{\boldsymbol{\omega}})^H\mathbf{x}}{\mathbf{m}(\widehat{\boldsymbol{\omega}})^H\mathbf{m}(\widehat{\boldsymbol{\omega}})} \\ \widehat{\boldsymbol{\omega}} = \arg\max_{\boldsymbol{\omega}'}\left\{\left\|\Pi_{\mathbf{m}(\boldsymbol{\omega}')}\mathbf{x}\right\|^2\right\} \\ \mathbf{x} = \alpha\boldsymbol{\mu}(\boldsymbol{\eta}) \end{cases}. \tag{16}$$

Then, through direct numerical computation of the MMLE without noise, one will obtain the pseudo-true parameters $\boldsymbol{\omega}_{pt}$ and α_{pt}. Also for relatively short coherent integration time and realistic acceleration, the following closed-form expressions have been derived (refer to Appendix A for the derivation details):

$$\alpha_{pt} \approx \alpha, \quad \tau_{pt} = \tau, \quad b_{pt} = b + dT_e, \quad \Delta b = b_{pt} - b = dT_e, \tag{17}$$

where T_e is the integration time, that is, the duration (support) of the baseband signal since we consider the narrowband assumption (see Appendix A). The above equations are valid for realistic scenarios but they are no longer applicable with high values of acceleration ($>$100 g, with g= 9.81 m/s^2) or extensive signal estimation intervals ($\gg$ 20 ms). On the other hand, it is well known that for the conditional signal model in this work, the MMLE converges asymptotically (at high SNR) to the pseudo-true values [24] with a covariance matrix equal to the MCRB. Thus, in the following section we derive a compact MCRB expression for joint time-delay and Doppler estimation.

5. A Compact MCRB for Joint Time-delay and Doppler Estimation

A general equation to compute the MCRB, represented with the Huber covariance [15, 24, 16], has been derived for specific types of parameterised distribution models. We can define the MCRB as:

$$\mathbf{MCRB}_{\boldsymbol{\theta}_{pt}} = \mathbf{A}(\boldsymbol{\theta}_{pt})^{-1}\mathbf{B}(\boldsymbol{\theta}_{pt})\mathbf{A}(\boldsymbol{\theta}_{pt})^{-1}, \tag{18}$$

where the matrices $\mathbf{A}(\boldsymbol{\theta}_{pt})$ and $\mathbf{B}(\boldsymbol{\theta}_{pt})$ depend on the pseudo-true parameters and the partial derivatives of the misspecified signal model. A simplification of the MCRB equation, that suits the models considered in this work, is given in the Slepian-Bangs form with a constant covariance w.r.t. estimated parameters [14],

$$\mathbf{B}(\boldsymbol{\theta}_{pt}) = \frac{2}{\sigma_n^2}\mathrm{Re}\left\{\left(\frac{\partial \alpha_{pt}\mathbf{m}(\boldsymbol{\omega}_{pt})}{\partial \boldsymbol{\theta}_{pt}}\right)^H \left(\frac{\partial \alpha_{pt}\mathbf{m}(\boldsymbol{\omega}_{pt})}{\partial \boldsymbol{\theta}_{pt}}\right)\right\}, \tag{19}$$

$$\begin{aligned}\mathbf{A}(\boldsymbol{\theta}_{pt}) &= -\frac{2}{\sigma_n^2}\mathrm{Re}\left\{\left(\frac{\partial \alpha_{pt}\mathbf{m}(\boldsymbol{\omega}_{pt})}{\partial \boldsymbol{\theta}_{pt}}\right)^H \left(\frac{\partial \alpha_{pt}\mathbf{m}(\boldsymbol{\omega}_{pt})}{\partial \boldsymbol{\theta}_{pt}}\right)\right\} + \frac{2}{\sigma_n^2}\mathrm{Re}\left\{(\delta\mathbf{m})^H\left(\frac{\partial^2 \alpha_{pt}\mathbf{m}(\boldsymbol{\omega}_{pt})}{\partial \boldsymbol{\theta}_{pt}\partial \boldsymbol{\theta}_{pt}^\top}\right)\right\}\\ &= \frac{2}{\sigma_n^2}\mathrm{Re}\left\{(\delta\mathbf{m})^H\left(\frac{\partial^2 \alpha_{pt}\mathbf{m}(\boldsymbol{\omega}_{pt})}{\partial \boldsymbol{\theta}_{pt}\partial \boldsymbol{\theta}_{pt}^\top}\right)\right\} - \mathbf{B}(\boldsymbol{\theta}_{pt}),\end{aligned} \tag{20}$$

where $\delta\mathbf{m} = \alpha\boldsymbol{\mu}(\boldsymbol{\eta}) - \alpha_{pt}\mathbf{m}(\boldsymbol{\omega}_{pt})$ is the difference between the means of the misspecified model and the true model. The computations of partial derivatives for the matrix $\mathbf{B}(\boldsymbol{\theta}_{pt})$ have been detailed in Appendix B, following the methodology of [10]. Actually, $\mathbf{B}(\boldsymbol{\theta}_{pt})$ is equivalent to the Fisher information matrix for a fully specified model with parameters $\boldsymbol{\theta}_{pt}$. By factorising the partial derivatives, we then express $\mathbf{B}(\boldsymbol{\theta}_{pt})$ in a matrix form

$$\mathbf{B}(\boldsymbol{\theta}_{pt}) = \frac{2f_s}{\sigma_n^2}\mathrm{Re}\left\{\mathbf{Q}\mathbf{W}\mathbf{Q}^H\right\}, \tag{21}$$

where

$$\mathbf{Q} = \begin{bmatrix} -j\rho_{pt} & 0 & 0 \\ -1 & 0 & 0 \\ -jw_c\rho_{pt}b_{pt} & 0 & \rho_{pt} \\ 0 & jw_c\rho_{pt} & 0 \end{bmatrix}, \quad \mathbf{W} = \begin{bmatrix} w_1 & w_2 & w_3^* \\ w_2 & W_{2,2} & W_{3,2}^* \\ w_3 & W_{3,2} & W_{3,3} \end{bmatrix}, \tag{22}$$

with $\mathbf{W}$ derived in [10] and also detailed in Appendix B to give the expressions w.r.t. the baseband signal samples. The product $\mathrm{Re}\left\{\mathbf{Q}\mathbf{W}\mathbf{Q}^H\right\}$ is presented in (23), which gives the terms required required to compute (21)),

$$\begin{bmatrix} w_1\rho^2 & 0 & \rho^2 w_c b w_1 - \rho^2\mathrm{Im}\{w_3\} & -\rho^2 w_c w_2 \\ 0 & w_1 & -\rho\mathrm{Re}\{w_3\} & 0 \\ \rho^2 w_c b w_1 - \rho^2\mathrm{Im}\{w_3\} & -\rho\mathrm{Re}\{w_3\} & w_c^2\rho^2 b^2 w_1 + \rho^2 W_{3,3} - 2w_c\rho^2 b\mathrm{Im}\{w_3\} & -w_c^2\rho^2 b w_2 + \rho^2 w_c\mathrm{Im}\{W_{3,2}\} \\ -\rho^2 w_c w_2 & 0 & -w_c^2\rho^2 b w_2 + \rho^2 w_c \mathrm{Im}\{W_{3,2}\} & w_c^2\rho^2 W_{2,2} \end{bmatrix}. \tag{23}$$

Now, we aim to derive the terms of the MCRB that come from the misspecified model. First, we compute the matrix $\mathbf{A}(\boldsymbol{\theta}_{pt})$. Based on the pseudo-true values in (17) obtained from the KLD minimisation, we can substitute the following equivalences: $\tau_{pt} = \tau$, $\alpha_{pt} = \alpha$, and $b_{pt} = b + dT_e$ into the misspecified signal model and find that

$$\delta\mathbf{m} = \rho_{pt}\left(e^{\Psi(t)} - 1\right)e^{-j\Phi_{pt}}s^H(t-\tau_{pt})e^{j\omega_c b_{pt}(t-\tau)}, \tag{24}$$

where $\Psi(t) = -j\omega_c(dT_e(t-\tau) - d(t-\tau)^2)$ (see Appendix C).

Secondly, the tedious computation of $\frac{\partial^2 \alpha_{pt}\mathbf{m}(\omega_{pt})}{\partial\boldsymbol{\theta}_{pt}\partial\boldsymbol{\theta}_{pt}^\top}$ is also detailed in Appendix C. Then, we compute the product,

$$(\delta\mathbf{m})^H \left(\frac{\partial^2 \alpha_{pt}\mathbf{m}(\boldsymbol{\omega}_{pt})}{\partial\boldsymbol{\theta}_{pt}\partial\boldsymbol{\theta}_{pt}^\top}\right) = \rho_{pt}\left(e^{\Psi(t)} - 1\right) e^{-j\Phi_{pt}} s^H(t-\tau) e^{j\omega_c b_{pt}(t-\tau)} \left(\frac{\partial^2 \alpha_{pt}\mathbf{m}(\boldsymbol{\omega}_{pt})}{\partial\boldsymbol{\theta}_{pt}\partial\boldsymbol{\theta}_{pt}^\top}\right). \tag{25}$$

The result above can be expanded into a matrix made up of common terms with $\mathbf{QWQ}^H$, and simplified as shown in Appendix C, leading to,

$$\mathbf{A}(\boldsymbol{\theta}_{pt}) \quad = \frac{2f_s\rho}{\sigma_n^2}\mathrm{Re}\left\{(\delta\mathbf{m})^H\left(\frac{\partial^2 \alpha_{pt}\mathbf{m}(\omega_{pt})}{\partial\boldsymbol{\theta}_{pt}\partial\boldsymbol{\theta}_{pt}^\top}\right) - \mathbf{QWQ}\right\} = \frac{2f_s\rho}{\sigma_n^2}\mathrm{Re}\left\{\boldsymbol{\chi}\right\}, \tag{26}$$

$$\begin{bmatrix} -w_{e_1}\rho & jw_{e_1} & -\rho w_c b w_{e_1} - j\rho w_{e_3} & \rho w_c w_{e_2} \\ jw_{e_1} & -\frac{w_1}{\rho} & jw_c b w_{e_1} - w_{e_3} & -jw_c w_{e_2} \\ -\rho w_c b w_{e_1} - j\rho w_{e_3} & jw_c b w_{e_1} - w_{e_3} & w_c^2\rho b^2 w_{e_1} + \rho w_{e_M} - 2jw_c\rho b\cdot w_{e_3} & w_c^2\rho b w_{e_2} + j\rho w_c w_{e_{3,2}} + j\rho w_c w_{e_1} \\ \rho w_c w_{e_2} & -jw_c w_{e_2} & w_c^2\rho b w_{e_2} + j\rho w_c w_{e_{3,2}} + j\rho w_c w_{e_1} & -\rho w_c^2 w_{e_{2,2}} \end{bmatrix} \tag{27}$$

Within matrix $\boldsymbol{\chi}$, the new terms w_e have not been previously computed. Following the same procedure as in [25, 10, 11] (detailed in Appendix D), these new terms can be resolved using properties of Fourier transforms. Matrix $\boldsymbol{\chi}$ can be decomposed into a similar combination of matrices as in (21), with some modifications to ensure the new matrix $\mathbf{W}_e$ includes the newly derived integrals as well as w_1. $\boldsymbol{\chi} = -\mathbf{Q}_e\mathbf{W}_e\mathbf{Q}_e^H$ with,

$$\mathbf{Q}_e = \begin{bmatrix} -j\rho & 0 & 0 & 0 & 0 \\ -1 & 1 & 0 & 0 & -1 \\ -j\rho\omega_c b & 0 & 0 & \rho & 0 \\ 0 & 0 & j\omega_c\rho & 0 & 0 \end{bmatrix}, \ \mathbf{W}_e = \begin{bmatrix} w_{e_1} & 0 & w_{e_2} & w_{e_3} & 0 \\ 0 & w_1 & 0 & 0 & 0 \\ w_{e_2} & 0 & W_{e_{2,2}} & W_{e_{2,3}} & 0 \\ w_{e_3} & 0 & W_{e_{3,2}} & w_{e_M} & 0 \\ 0 & 0 & 0 & 0 & w_{e_1} \end{bmatrix} \tag{28}$$

These relatively simple matrices are more convenient to implement than (27). Then with this closed-form, the MCRB for a specific signal can be simply computed using only the signal samples.

6. Validation and Discussion

The matrices derived above are computed using synthetically generated GPS L1 C/A signal samples without noise. The validation of our closed form equations is possible by observing the convergence of the appropriate estimator's MSE to the associated bounds under different levels of noise. To that extent, we have setup Monte Carlo simulations that will provide the estimation performance of an MLE assuming the misspecified model defined above. The simulations include the generated signals, which have the true propagation effects of delay, Doppler, and acceleration applied. The misspecified estimator (MMLE) is created by searching for the MLE solutions for only delay and Doppler. The MSE of the delay and Doppler parameters are the only values analysed as they are of primary interest for navigation applications. We choose different integration times and magnitudes of acceleration to apply on the true signal as these parameters are seen to directly effect the Doppler bias. Only high dynamics scenarios with ($|\mathbf{a}| \geq 50g$ [1, Chapter 32]) are considered in the analysis. The results are still relevant for low acceleration targets that result in lower Δb. The tested integration times do not exceed 20 ms to fit within standard GNSS values and satisfy the constraint derived in (A.23). We expect the true MSE of an MMLE to converge to Δb^2+MCRB at the high SNR regime [24], i.e., the bound for the misspecified estimator is a combination of the parameter bias and minimum variance provided by the MCRB. The true MSE refers to the error of the misspecified estimate w.r.t. its corresponding true value ($\sqrt{\mathrm{MSE}_b}$ MMLE w.r.t. b_{true}, light-blue dashed cross). Note also that the MSE of the misspecified estimate w.r.t. the associated pseudo-true value ($\sqrt{\mathrm{MSE}_b}$ MMLE w.r.t. b_{pt}, orange dashed plus) is expected to converge to the MCRB [13, 24, 15]. The signal parameters we analyze are delay and Doppler because they are more important for navigation purposes. The impact of misspecification bias would be greater for delay and Doppler than if the amplitude or phase are biased by the acceleration. The misspecified delay estimation is seen in Fig. 1 to converge to the same bound as the fully specified case. Fig. 1 also shows that the magnitude of acceleration has no effect on the asymptotic MSE. Additional simulations can be made to observe an equivalent independence from integration time.

Fig. 2 shows that the MMLE has its true MSE (light-blue dashed cross) converge to the Δb^2+MCRB curve (green circles) and remains below the fully specified CRB (red diamonds) for a significant window of SNR values. The MSE convergence of the misspecified estimator validates the closed forms of the MCRB and Δb. It is also seen that the MSE of the fully specified estimator (magenta stars) converges to the fully specified bound, so we can analyse the differences in magnitudes between each specification model. Fig. 2 shows that for short observation intervals of the signal, even a high dynamics scenario does not benefit from a fully specified model until SNR values greater than 33 dB are achieved. Typical, every-day tracking scenarios (usually with SNR $\geq$25 dB [26]) do not reach an acceleration as high as 50g, so lower Δb is expected and the best receiver architecture to choose in general would be the misspecified delay-Doppler estimation model. This result is an example of the trade-off between the systematic error introduced by misspecification and the variance increase due to including an extra parameter to be estimated. It is not immediately apparent that improving the specification of a signal model for high dynamics can cause a loss in performance. In general, we can already say the inclusion of acceleration estimation is not necessary for applications which experience low magnitude accelerations.

We would now like to see a case where inclusion of acceleration estimation is advantageous. For certain SNR values where Δb^2+MCRB (green circles) has higher magnitude than the fully specified bound (red diamonds), it can be considered worth including the acceleration estimation. This goes into the niche

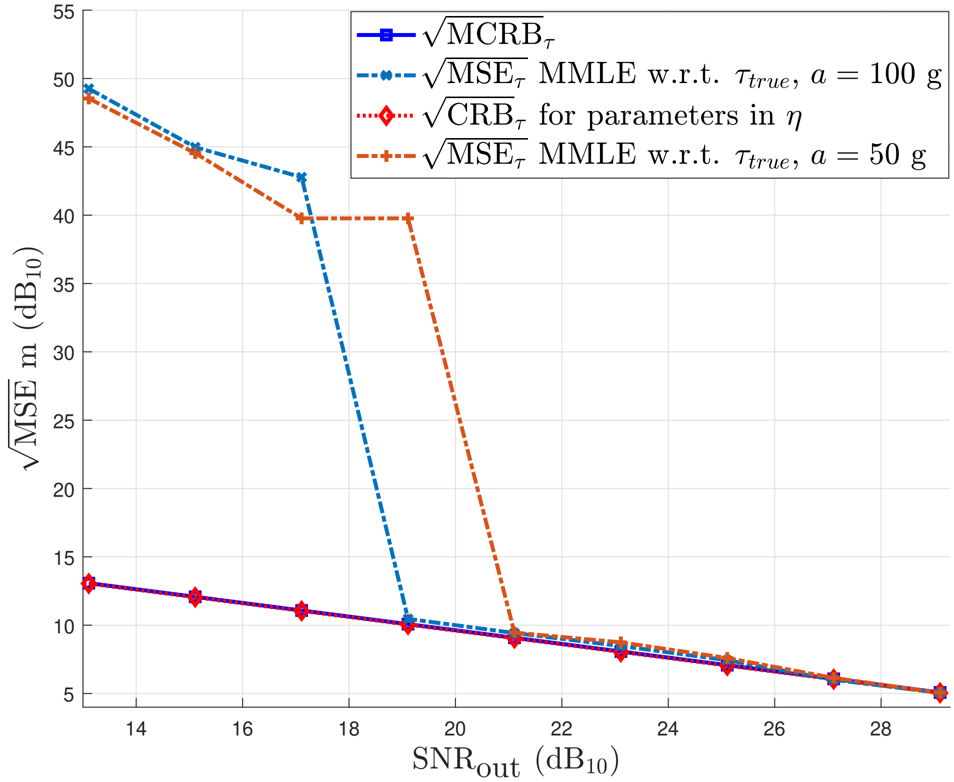

Figure 1: MCRB and MSE for the misspecified MLE of the time-delay parameter with respect to true time-delay value (accelerations = 50 and 100g, duration = 10 ms).

classification of high dynamics scenarios with limited SNR. A real-world application to consider can be tracking of objects entering the Earth's atmosphere such as large spacecraft or intercontinental ballistic missiles. These targets experience a very high magnitude negative acceleration due to drag forces and can be susceptible to interferences, either natural ionisation or synthetic jamming. There can be an upper limit of approximately 100 g of instantaneous acceleration considered for ballistic atmospheric reentry, a scenario that represents some of the highest dynamics observable [27]. In limited SNR scenarios, it makes sense that the integration time of the signal is increased. As well as acceleration, a longer signal duration contributes to increasing the magnitude Δb as it is shown in (17). Hence, the next scenario considers double the acceleration and double the integration time. Fig. 3 shows the convergence of the MSE to the appropriate bounds. For an acceleration of 100g, Doppler frequency set to 10 kHz and signal duration of 10 ms, the region where a misspecified estimation is preferred has been reduced.

The magnitude of the bounds are decreased for all SNR by increasing the integration time; however, Δb also increases because it is proportional to the integration time. This effect is seen in Fig. 3, where the

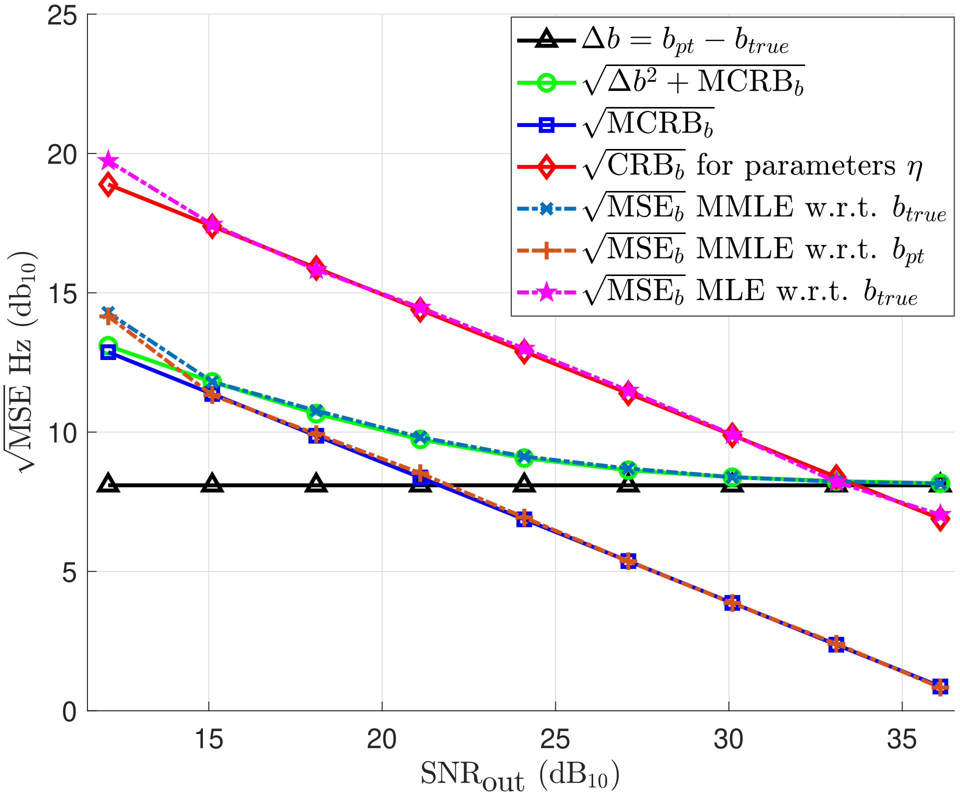

Figure 2: MCRB and MSE for misspecified ML Doppler estimator with respect to true and pseudo-true Doppler and the convergence to appropriate bounds (acceleration = 50g, duration = 5 ms).

acceleration and integration time are both doubled, resulting in a 6 dB increase of the Δb while the CRB and the MCRB have both decreased by 3 dB. Hence, increasing the integration time will both increase the true MSE of the MMLE and improve the fully specified bound enough that it becomes worth including estimation of acceleration. In the case of Fig. 3, the fully specified CRB is preferred for SNR values higher than 15 dB, which involves the entire GPS C/A operational system [28]. Another example of misspecified Doppler estimation is shown in Fig. 4, where the integration time has been taken to the limits of GNSS operations and the acceleration magnitude has been reduced to a relatively low value. This case indicates that even the less extreme cases of acceleration have a noticeable effect on the Doppler estimation when the integration time is high enough. The SNR threshold where it is preferable to use the fully specified estimator is at approximately 29 dB, again within a realistic operating range. This presents a similar scenario to Fig. 2, where the misspecified estimator achieves better MSE performance for low SNR values due to the bias being less extreme than the demand of an additional estimated parameter.

Finally, we present results of the MSE of the Doppler MMLE as a function of acceleration and fixing

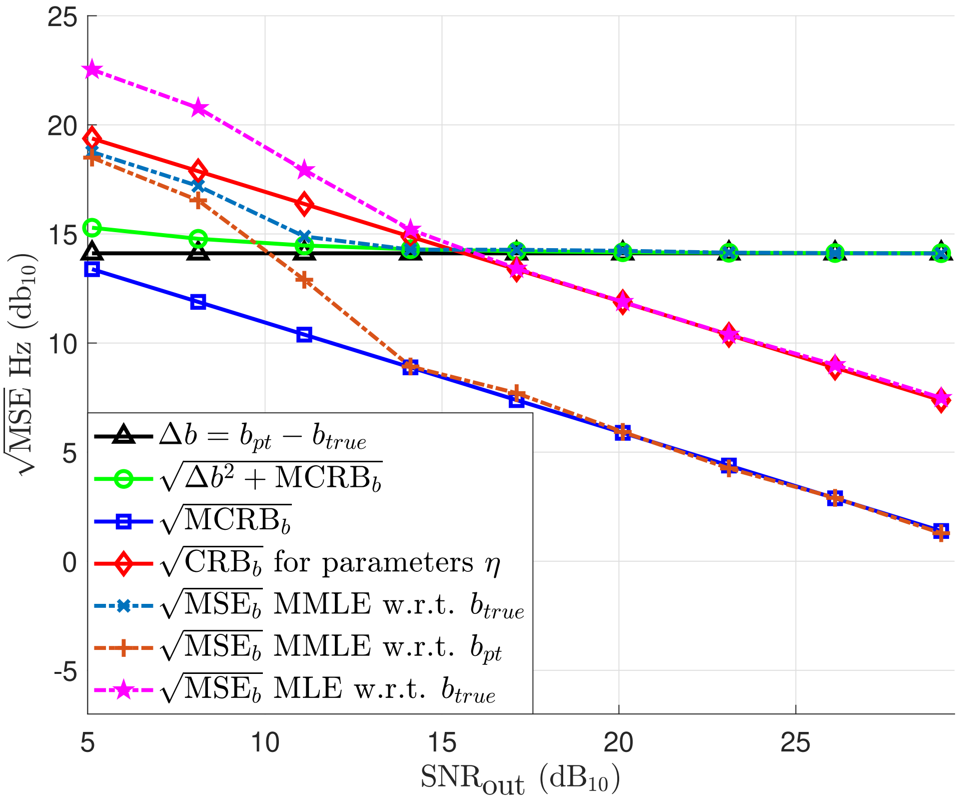

Figure 3: MCRB and MSE for misspecified ML Doppler estimator with respect to true and pseudo-true Doppler and the convergence to appropriate bounds (acceleration = 100g, duration = 10 ms).

the SNR_{OUT} = 25dB in Figure 5. This allows visualisation of the acceleration threshold at which the fully specified estimator is preferred in realistic noise environment. Figure 5 suggests that the threshold is at 32 g for a signal integration time of 10 ms. We can expect this threshold to be lower for higher integration times based on the relation presented in Equation (15) for Δb.

Hence, specific scenarios exist where the use of the fully specified MLE is convenient and others where the MMLE is more optimal. It is easy to recompute these bounds and compare for different signals, acceleration values, and integration times since this work has provided compact formulations of the MCRB and Δb. All that is needed are synthetic signal samples and the true values of delay, Doppler, and acceleration. An easy method to decide which of the parameterizations should be used for a specific application of Doppler estimation is to:

- Determine the limiting (or expected) values for acceleration and integration time.
- Calculate the closed-form expressions of the MCRB and Δb.

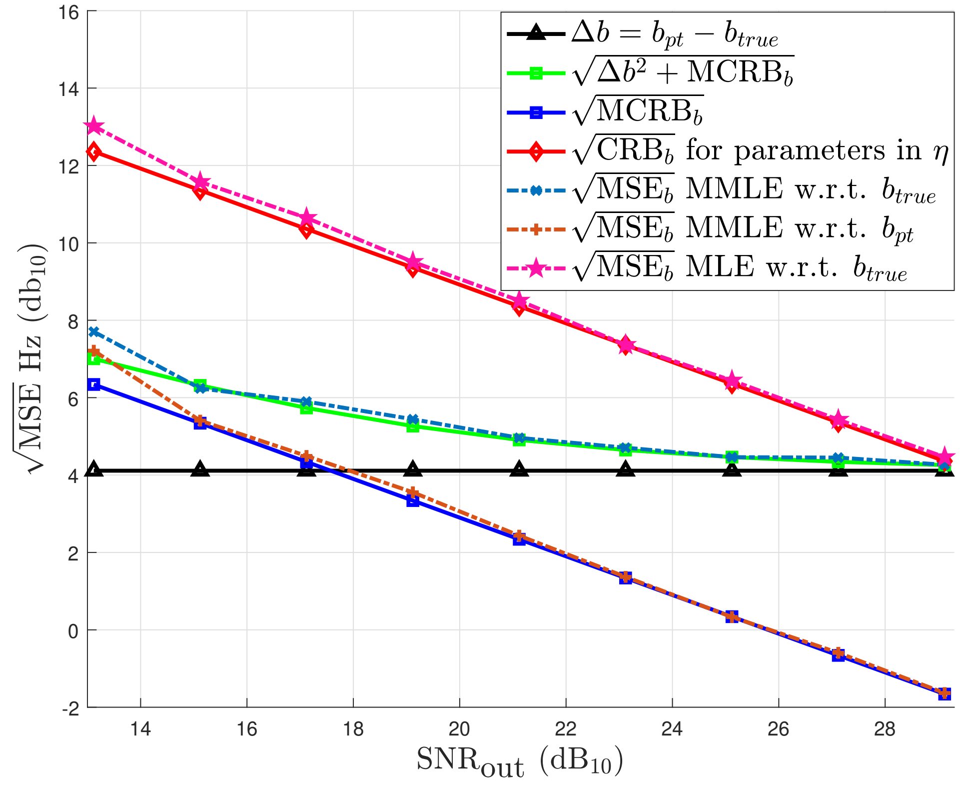

Figure 4: MCRB and MSE for misspecified MLE of the Doppler parameter with respect to true and pseudo-true values (acceleration = 5g, duration = 20 ms).

- Find the fully specified CRB using [11].
- If the intersection point between the CRB and the Δb^2+MCRB is within your field of operational SNR values, use the matched filter
- Otherwise, use the mismatched filter that neglects acceleration.

7. Conclusion

This work derived compact closed-form expressions of the misspecified CRB and pseudo-true parameters of time-delay and Doppler for a high dynamics signal model. The results of this work provide an insight into the decisions for defining the parameterisation of a signal model. For most of the realistic scenarios with non-zero acceleration and short integration times, the misspecified MLE Doppler estimation can be reduced in the MSE sense at the cost of a systematic error induced in the true parameter estimation. On the other hand, certain limits cases were found, such as an acceleration magnitude of 100g and integration time

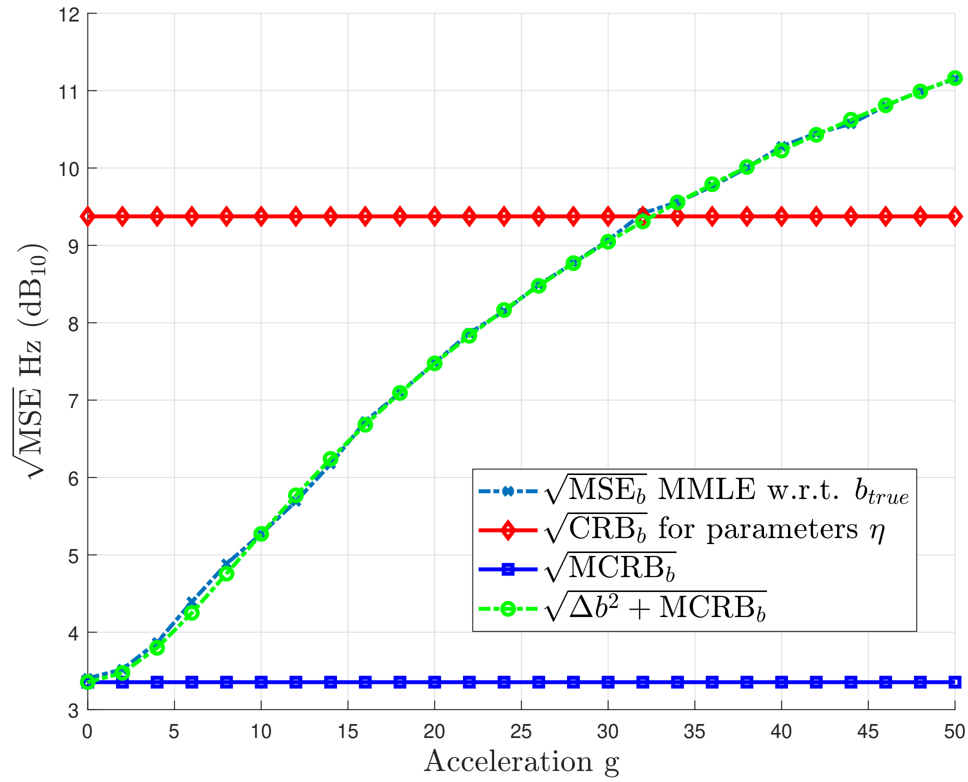

Figure 5: MCRB and MSE of the misspecified MLE of the Doppler parameter at SNR_{OUT} = 25 dB as a function of the acceleration (duration = 10 ms).

of 10 ms, where the MLE estimator including the acceleration estimation achieves a lower MSE for SNR higher than ≥15 dB. At this point the well specified MLE converges to the CRB including acceleration and avoids the larger systematic error Δb due to the high dynamics. The fact that two different architectures with asymptotic performance limits that change from scenario to scenario validates the need to calculate the theoretical limits presented in this article, in order to decide which is the optimal estimator, in the MSE sense, for each particular scenario.

Acknowledgements

Partially supported by DGA/AID projects 2019.65.0068.00.470.75.01 and 2021.65.0070.00.470.75.01.

Appendix A. Pseudo-True Parameter Derivation

This appendix includes the expansion of the KLD equation and consequently the minimization process to derive the pseudo-true parameters. It is seen that the pseudo-true parameters for delay and Doppler

($\boldsymbol{\omega}_{pt}$) require a further maximization process, which is also detailed in this Appendix.

$$E_p\left[-lnf_{\boldsymbol{\epsilon}'}\right] = -Nln(\pi) - 2Nln(\sigma_n) + \frac{1}{\sigma_n^2}E_p\begin{bmatrix}(\mathbf{x}-\alpha\boldsymbol{\mu}(\boldsymbol{\eta})+\alpha\boldsymbol{\mu}(\boldsymbol{\eta})-\alpha'\mathbf{m}(\boldsymbol{\omega}'))^H\\ \cdot(\mathbf{x}-\alpha\boldsymbol{\mu}(\boldsymbol{\eta})+\alpha\boldsymbol{\mu}(\boldsymbol{\eta})-\alpha'\mathbf{m}(\boldsymbol{\omega}'))\end{bmatrix}. \tag{A.1}$$

To minimise (A.1) w.r.t. the argument $\boldsymbol{\theta}'$, the equation can be simplified as,

$$\begin{aligned}
&\arg\min_{\boldsymbol{\theta}'}\left\{E_p\left[-lnf_{\boldsymbol{\epsilon}'}(\mathbf{x};\boldsymbol{\epsilon}')\right]\right\}\\
=\;&\arg\min_{\boldsymbol{\theta}'}\left\{E_p\begin{bmatrix}(\mathbf{x}-\alpha\boldsymbol{\mu}(\boldsymbol{\eta}))^H(\mathbf{x}-\alpha\boldsymbol{\mu}(\boldsymbol{\eta}))\\ +(\mathbf{x}-\alpha\boldsymbol{\mu}(\boldsymbol{\eta}))^H(\alpha\boldsymbol{\mu}(\boldsymbol{\eta})-\alpha'\mathbf{m}(\boldsymbol{\omega}'))\\ +(\alpha\boldsymbol{\mu}(\boldsymbol{\eta})-\alpha'\mathbf{m}(\boldsymbol{\omega}'))^H(\mathbf{x}-\alpha\boldsymbol{\mu}(\boldsymbol{\eta}))\\ +(\alpha\boldsymbol{\mu}(\boldsymbol{\eta})-\alpha'\mathbf{m}(\boldsymbol{\omega}'))^H(\alpha\boldsymbol{\mu}(\boldsymbol{\eta})-\alpha'\mathbf{m}(\boldsymbol{\omega}'))\end{bmatrix}\right\}\\
=\;&\arg\min_{\boldsymbol{\theta}'}\left\{(\alpha\boldsymbol{\mu}(\boldsymbol{\eta})-\alpha'\mathbf{m}(\boldsymbol{\omega}'))^H(\alpha\boldsymbol{\mu}(\boldsymbol{\eta})-\alpha'\mathbf{m}(\boldsymbol{\omega}'))\right\}\\
=\;&\arg\min_{\boldsymbol{\theta}'}\left\{\|\alpha\boldsymbol{\mu}(\boldsymbol{\eta})-\alpha'\mathbf{m}(\boldsymbol{\omega}')\|^2\right\}.
\end{aligned}\tag{A.2}$$

We define the orthogonal projector $\Pi_{\mathbf{A}}^{\perp} = \mathbf{I} - \Pi_{\mathbf{A}}$ with $\Pi_{\mathbf{A}} = \mathbf{A}\left(\mathbf{A}^H\mathbf{A}\right)^{-1}\mathbf{A}^H$, which leads to

$$\begin{aligned}
&\|\alpha\boldsymbol{\mu}(\boldsymbol{\eta})-\alpha'\mathbf{m}(\boldsymbol{\omega}')\|^2 = \left\|\left(\Pi_{\mathbf{m}(\boldsymbol{\omega}')}+\Pi_{\mathbf{m}(\boldsymbol{\omega}')}^{\perp}\right)(\alpha\boldsymbol{\mu}(\boldsymbol{\eta})-\alpha'\mathbf{m}(\boldsymbol{\omega}'))\right\|^2\\
&= \left\|\Pi_{\mathbf{m}(\boldsymbol{\omega}')}(\alpha\boldsymbol{\mu}(\boldsymbol{\eta})-\alpha'\mathbf{m}(\boldsymbol{\omega}'))\right\|^2 + \left\|\Pi_{\mathbf{m}(\boldsymbol{\omega}')}^{\perp}(\alpha\boldsymbol{\mu}(\boldsymbol{\eta})-\alpha'\mathbf{m}(\boldsymbol{\omega}'))\right\|^2\\
&= \left\|\Pi_{\mathbf{m}(\boldsymbol{\omega}')}\alpha\boldsymbol{\mu}(\boldsymbol{\eta})-\alpha'\mathbf{m}(\boldsymbol{\omega}')\right\|^2 + \left\|\Pi_{\mathbf{m}(\boldsymbol{\omega}')}^{\perp}\alpha\boldsymbol{\mu}(\boldsymbol{\eta})\right\|^2\\
&= \left\|\mathbf{m}(\boldsymbol{\omega}')\left(\frac{\mathbf{m}(\boldsymbol{\omega}')^H\alpha\boldsymbol{\mu}(\boldsymbol{\eta})}{\mathbf{m}(\boldsymbol{\omega}')^H\mathbf{m}(\boldsymbol{\omega}')}-\alpha'\right)\right\|^2 + \left\|\alpha\boldsymbol{\mu}(\boldsymbol{\eta})-\Pi_{\mathbf{m}(\boldsymbol{\omega}')}\alpha\boldsymbol{\mu}(\boldsymbol{\eta})\right\|^2,
\end{aligned}\tag{A.3}$$

We continue the derivation from (15) to develop the equation for $\boldsymbol{\omega}_{pt}$. The goal is to derive the equations for the pseudo-true delay and Doppler in a form that depends on the true parameters.

$$\boldsymbol{\omega}_{pt} = \arg\max_{\boldsymbol{\omega}'}\left\{\left\|\Pi_{\mathbf{m}(\boldsymbol{\omega}')}\alpha\boldsymbol{\mu}(\boldsymbol{\eta})\right\|^2\right\} \tag{A.4}$$

$$\left\|\Pi_{\mathbf{m}(\boldsymbol{\omega})}\alpha\boldsymbol{\mu}(\boldsymbol{\eta})\right\|^2 = (\alpha\boldsymbol{\mu}(\boldsymbol{\eta}))^H\,\Pi_{\mathbf{m}(\boldsymbol{\omega})}\,(\alpha\boldsymbol{\mu}(\boldsymbol{\eta})), \tag{A.5}$$

$$\left\|\Pi_{\mathbf{m}(\boldsymbol{\omega})}\alpha\boldsymbol{\mu}(\boldsymbol{\eta})\right\|^2 = \frac{(\alpha\boldsymbol{\mu}(\boldsymbol{\eta}))^H\mathbf{m}(\boldsymbol{\omega})\mathbf{m}(\boldsymbol{\omega})^H\,(\alpha\boldsymbol{\mu}(\boldsymbol{\eta}))}{\mathbf{m}(\boldsymbol{\omega})^H\mathbf{m}(\boldsymbol{\omega})}. \tag{A.6}$$

(A.6) can now be presented as a squared value. The sampling period T_s is also included for later conversion to an integral,

$$\left|\frac{\mathbf{m}(\boldsymbol{\omega})^H\,(\alpha\boldsymbol{\mu}(\boldsymbol{\eta}))}{\sqrt{\mathbf{m}(\boldsymbol{\omega})^H\mathbf{m}(\boldsymbol{\omega})}}\right|^2 = \left|\frac{\frac{1}{T_s}\mathbf{m}(\boldsymbol{\omega})^H\,(\alpha\boldsymbol{\mu}(\boldsymbol{\eta}))\,T_s}{\frac{1}{\sqrt{T_s}}\sqrt{\mathbf{m}(\boldsymbol{\omega})^H\mathbf{m}(\boldsymbol{\omega})T_s}}\right|^2. \tag{A.7}$$

For conciseness in equations, we denote the received signal after some delay τ as $s_\tau = s(t-\tau)$. Moreover, note that it is simple to verify from the MMLE in a noiseless environment considering short signal length (in the order of the 10-20 ms) and accelerations in the order of the 50 g that $\frac{\mathbf{m}(\omega_{pt})^H \boldsymbol{\mu}(\boldsymbol{\eta})}{\mathbf{m}(\omega_{pt})^H \mathbf{m}(\omega_{pt})} \approx 1$. Then for those particular scenarios we can set $\alpha_{pt} \approx \alpha$. We expand (A.7) to obtain the following

$$\left\|\Pi_{\mathbf{m}(\omega)} \alpha \boldsymbol{\mu}(\boldsymbol{\eta})\right\|^2 = \frac{|\alpha|^2}{T_s} \left| \frac{\int_{-\infty}^{+\infty} s_{\tau_{pt}}^* s_\tau e^{j\omega_c (b_{pt}(t-\tau_{pt}) - b(t-\tau) - d(t-\tau)^2)} dt}{\sqrt{\int_{-\infty}^{+\infty} \left|s_{\tau_{pt}}\right|^2 dt}} \right|^2. \tag{A.8}$$

We say that $\int_{-\infty}^{+\infty} |s(t)|^2 \, dt = E$, the energy of the signal and we shift the integration variable from t to $(t-\tau)$ with τ constant. The difference between the true and pseudo-true parameters, giving the respective misspecification errors are $\Delta\tau = \tau_{pt} - \tau$, and $\Delta b = b_{pt} - b$. We substitute these values to continue the simplification of (A.8), obtaining,

$$\left\|\Pi_{\mathbf{m}(\omega)} \alpha \boldsymbol{\mu}(\boldsymbol{\eta})\right\|^2 = \frac{|\alpha|^2}{T_s \sqrt{E}} \left| \int_{-\infty}^{+\infty} s_{\Delta\tau}^* s_0 e^{j\omega_c (\Delta b t - d t^2)} e^{-j\omega_c b_{pt} \Delta\tau} dt \right|^2. \tag{A.9}$$

The assumption $\Delta\tau = 0$ is made based on results from numerical computation of τ_{pt}. The numerical computation was conducted by simultaneously finding the τ and b values that maximise (A.7), τ_{pt} was found to be approximately equal to the true delay τ,

$$\left\|\Pi_{\mathbf{m}(\omega)} \alpha \boldsymbol{\mu}(\boldsymbol{\eta})\right\|^2 = \frac{|\alpha|^2}{T_s \sqrt{E}} \left| \int_{-\infty}^{+\infty} s_{\Delta\tau}^* s_0 e^{j\omega_c (\Delta b t - d t^2)} dt \right|^2. \tag{A.10}$$

The time interval over which to integrate is shifted to the total time of the signal observation T_e.

$$\left\|\Pi_{\mathbf{m}(\omega)} \alpha \boldsymbol{\mu}(\boldsymbol{\eta})\right\|^2 = \frac{|\alpha|^2}{T_s \sqrt{E}} \left| \int_0^{T_e} s_{\Delta\tau}^* s_0 e^{j\phi(t; b', b, d)} dt \right|^2, \tag{A.11}$$

$$\phi\left(t; b_{pt}, b, d\right) = \omega_c \left(\Delta b t - d t^2 - C_I\right). \tag{A.12}$$

Where C_I is a definite integral in $\phi(t; b_{pt}, b, d)$, which gives an arbitrary integration constant and is removed whenever taking the square of the norm by multiplying conjugates of complex exponentials. We compute the definite integral in a closed-form to obtain $C_I = \frac{1}{T_e} \int_0^{T_e} \left(\Delta b t - d t^2\right) dt = \frac{1}{T_e} \left[\Delta b \frac{t^2}{2} - d \frac{t^3}{3}\right]_0^{T_e} \Rightarrow C_I = \Delta b \frac{T_e}{2} - d \frac{T_e^2}{3}$. Since the objective is to maximise (A.5) w.r.t. the pseudo-true parameters, we note the upper bound of the integral in (A.11) is the point that it equals the signal energy:

$$\left| \int_0^{T_e} s_{\Delta\tau}^* s_0 e^{j\phi\left(t; b_{pt}, b, d\right)} dt \right|^2 \leq E, \tag{A.13}$$

$$\int_0^{T_e} \left|s_{\Delta\tau}^*\right|^2 dt \int_0^{T_e} \left|s_0 e^{j\phi\left(t; b_{pt}, b, d\right)}\right|^2 dt \leq \left(\int_0^{T_e} |s_0|^2 \, dt \right)^2. \tag{A.14}$$

Equality only holds for (A.14) when the complex exponential has the exponent go to zero. This means we can define another function, which we aim to minimise instead of maximise.

$$\sigma_\phi^2\left(b_{pt}, b, d\right) = \frac{1}{T_e} \int_0^{T_e} \phi\left(t; b_{pt}, b, d\right)^2 dt, \tag{A.15}$$

$$\sigma_\phi^2 = \omega_c^2 \left(\frac{1}{T_e} \int_0^{T_e} \left(\left(\Delta b t - d t^2\right)^2 \right) dt - \left(C_I\right)^2 \right). \tag{A.16}$$

Solving the remaining integral in σ_ϕ^2 and simplifying,

$$\frac{1}{T_e}\int_0^{T_e}\left(\left(\Delta bt - dt^2\right)^2\right)dt = \Delta b^2\frac{T_e^2}{3} + d^2\frac{T_e^4}{5} - 2d\Delta b\frac{T_e^3}{4}. \tag{A.17}$$

Now, substituting $\boldsymbol{C_I}$ and (A.17) into (A.16) and simplifying,

$$\frac{\sigma_\phi^2\left(b_{pt}, b, d\right)}{\omega_c^2} = \frac{T_e^2}{12}\left((\Delta b - dT_e)^2 + d^2T_e^2\frac{3}{45}\right). \tag{A.18}$$

Finally, we see the value of the Doppler parameter that minimises (A.16) and hence maximises (15),

$$\sigma_\phi^2\left(b_{pt}, b, d\right) = \omega_c^2\frac{T_e^2}{12}\left(\left(b_{pt} - (b + dT_e)\right)^2 + d^2T_e^2\frac{3}{45}\right)$$

$$\Downarrow$$

$$\arg\min_{b_{pt}}\left\{\sigma_\phi^2\left(b_{pt}, b, d\right)\right\} = b + dT_e. \tag{A.19}$$

By substituting the solution for b_{pt} back into (A.16), we can see the dependence on d and T_e,

$$\sigma_\phi^2\left(b + dT_e, b, d\right) = \left(\omega_c dT_e^2\right)^2\frac{1}{220} = \left(\frac{a}{\lambda_c}T_e^2\right)^2\frac{\pi^2}{220}. \tag{A.20}$$

For this solution to be appropriate, we need the exponential in (A.14) to approach 1. We see from (A.15) that for $\sigma_\phi^2\left(b + dT_e, b, d\right) \ll 1 \Rightarrow \left|\phi\left(t; b + dT_e, b, d\right)\right| \ll 1$. This means that with the computed value of pseudo-true Doppler, the upper bound of (A.14) is met with,

$$\left|\int_0^{T_e} s_{\Delta\tau}^* s_0 e^{j\phi\left(t; b_{pt}, b, d\right)}dt\right|^2 \simeq \left|\int_0^{T_e} s_{\Delta\tau}^* s_0 dt\right|^2. \tag{A.21}$$

Equating (A.21) to the signal energy obtains the value of $\Delta\tau = 0$ that consequently maximises (15),

$$\arg\max_{\tau_{pt}}\left\{\left\|\Pi_{\mathbf{m}(\omega)}\alpha\boldsymbol{\mu}(\boldsymbol{\eta})\right\|^2\right\} = \tau. \tag{A.22}$$

The maximisation of this term is dependant on the assumption that $\sigma_\phi^2 \ll 1$. Therefore, the expressions for pseudo-true delay and Doppler can be stated under a certain condition on the acceleration and integration time. We can substitute realistic but high magnitudes into (A.20) to see if the condition is satisfied in true applications. We take $a = 100$ g and $T_e = 20$ ms to consider a high dynamic scenario with the maximum coherent integration time for GNSS signal processing. The condition is true for realistic magnitudes of acceleration or T_e.

$$\left(\frac{|a|}{\lambda_c}T_e^2\right)\frac{\pi}{\sqrt{220}} \ll 1 \Rightarrow \begin{cases} \tau'_{pt} = \tau \\ b'_{pt} = b + dT_e \end{cases}. \tag{A.23}$$

Appendix B. Computation of $\mathbf{B}(\boldsymbol{\theta}_{pt})$

The first degree partial derivatives have been previously defined [10]. They are presented again in this appendix for completeness of the results for the closed-form MCRB, which also requires these computations.

$$\frac{\partial \alpha_{pt}\mathbf{m}(\boldsymbol{\omega}_{pt})}{\partial \boldsymbol{\theta}_{pt}} = \begin{bmatrix} \frac{\partial \alpha_{pt}\mathbf{m}(\omega_{pt})}{\partial \rho_{pt}} & \frac{\partial \alpha_{pt}\mathbf{m}(\omega_{pt})}{\partial \Phi_{pt}} & \frac{\partial \alpha_{pt}\mathbf{m}(\omega_{pt})}{\partial \tau_{pt}} & \frac{\partial \alpha_{pt}\mathbf{m}(\omega_{pt})}{\partial b_{pt}} \end{bmatrix}, \tag{B.1}$$

$$\frac{\partial \alpha_{pt}\mathbf{m}(\boldsymbol{\omega}_{pt}))}{\partial \rho_{pt}} = e^{j\Phi_{pt}} s(t-\tau_{pt}) e^{-j\omega_c b_{pt}(t-\tau_{pt})},$$

$$\frac{\partial \alpha_{pt}\mathbf{m}(\boldsymbol{\omega}_{pt})}{\partial \Phi_{pt}} = j\rho_{pt} e^{j\Phi_{pt}} s(t-\tau_{pt}) e^{-j\omega_c b_{pt}(t-\tau_{pt})},$$

$$\frac{\partial \alpha_{pt}\mathbf{m}(\boldsymbol{\omega}_{pt})}{\partial \tau_{pt}} = -\rho_{pt} e^{j\Phi_{pt}} s^{(1)}(t-\tau_{pt}) e^{-j\omega_c b_{pt}(t-\tau_{pt})} + j\omega_c b_{pt} \rho_{pt} e^{j\Phi_{pt}} s(t-\tau_{pt}) e^{-j\omega_c b_{pt}(t-\tau_{pt})},$$

$$\frac{\partial \alpha_{pt}\mathbf{m}(\boldsymbol{\omega}_{pt})}{\partial b_{pt}} = -j\omega_c (t-\tau_{pt}) \rho_{pt} e^{j\Phi_{pt}} s(t-\tau_{pt}) e^{-j\omega_c b_{pt}(t-\tau_{pt})}.$$

The matrix $\mathbf{W}$ contains more previously computed terms that should be defined due to their appearance in $\mathbf{B}(\boldsymbol{\theta}_{pt})$ and hence the MCRB. These integrals are shown to be closed form and dependant only on the signal samples.

$$w_1 = \int_{-\infty}^{\infty} |s(t;\boldsymbol{\eta})|^2 \, dt = \frac{1}{f_s} \mathbf{s}^H \mathbf{s}, \; w_2 = \int_{-\infty}^{\infty} (t-\tau) \, |s(t;\boldsymbol{\eta})|^2 \, dt = \frac{1}{f_s^2} \mathbf{s}^H \mathbf{D} \mathbf{s}, \tag{B.2}$$

$$w_3 = \int_{-\infty}^{\infty} s^{(1)}(t;\boldsymbol{\eta}) s(t;\boldsymbol{\eta}) dt = \mathbf{s}^H \boldsymbol{\Lambda} \mathbf{s}, \; W_{3,3} = \int_{-\infty}^{\infty} \left| s^{(1)}(t;\boldsymbol{\eta}) \right|^2 dt = f_s \mathbf{s}^H \mathbf{V} \mathbf{s}, \tag{B.3}$$

$$W_{2,2} = \int_{-\infty}^{\infty} (t-\tau)^2 \, |s(t;\boldsymbol{\eta})|^2 \, dt = \frac{1}{f_s^3} \mathbf{s}^H \mathbf{D}^2 \mathbf{s}, \; W_{3,2} = \int_{-\infty}^{\infty} (t-\tau) s^{(1)}(t;\boldsymbol{\eta}) s^*(t;\boldsymbol{\eta}) dt = \frac{1}{f_s} \mathbf{s}^H \mathbf{D} \boldsymbol{\Lambda} \mathbf{s}, \tag{B.4}$$

with

$$\mathbf{D} = diag([N_1, N_1+1, ..., N_2-1, N_2]), \tag{B.5}$$

$$(\mathbf{V})_{n,n'} = \left| \begin{array}{l} n' \neq n : (-1)^{\left|n-n'\right|} \frac{2}{(n-n')^2} \\ \\ n' = n : \frac{\pi^2}{3} \end{array} \right., \; (\boldsymbol{\Lambda})_{n,n'} = \left| \begin{array}{l} n' \neq n : \frac{(-1)^{\left|n-n'\right|}}{(n-n')} \\ \\ n' = n : 0 \end{array} \right., \tag{B.6}$$

and $s^{(1)}(t)$ the first derivative of the signal $s(t)$. The methodology of this appendix is repeated with more complicated derivatives and integrals to compute the new closed-form MCRB.

Appendix C. Computation of $\mathbf{A}(\boldsymbol{\theta}_{pt})$

The matrix $\mathbf{A}(\boldsymbol{\theta}_{pt})$ is component of the MCRB that takes into account the misspecification. The first term to derive is $\delta\mathbf{m}$, which depends on the difference between the means of the misspecified signal model and the model including acceleration.

$$\begin{aligned}\delta\mathbf{m} &= \alpha s(t-\tau)e^{-j\omega_c(b(t-\tau)+d(t-\tau)^2)} - \alpha_{pt}s(t-\tau_{pt})e^{-j\omega_c b_{pt}(t-\tau_{pt})} \\ &= \alpha s(t-\tau)\left(e^{-j\omega_c(b(t-\tau)+d(t-\tau)^2)} - e^{-j\omega_c(b+dT_e))(t-\tau)}\right) \\ &= \alpha s(t-\tau)e^{-j\omega_c(b+dT_e)(t-\tau)}\left(e^{j\omega_c(dT_e(t-\tau)-d(t-\tau)^2)} - 1\right) \\ &= \rho_{pt}e^{j\Phi_{pt}}s(t-\tau)e^{-j\omega_c b_{pt}(t-\tau)}\left(e^{j\omega_c(dT_e(t-\tau)-d(t-\tau)^2)} - 1\right).\end{aligned} \tag{C.1}$$

The first derivatives w.r.t each parameter have been computed in (B.1). The process of going from each of these first derivatives to the following second derivatives is simple but results in too many equations to keep in the main body of this article. Therefore, this Appendix is a list of the second derivatives that have been substituted into (C.2). As the equations for $\mathbf{A}(\boldsymbol{\theta}_{pt})$ and $\mathbf{B}(\boldsymbol{\theta}_{pt})$ involve multiplication of complex conjugates, it is useful to note that every non-zero derivative includes a common complex exponential. The same complex exponential has been factored in (C.1) to simplify through conjugate multiplication. This common factor is therefore removed from the final form of the MCRB.

$$\frac{\partial^2\alpha_{pt}\mathbf{m}(\omega_{pt})}{\partial\boldsymbol{\theta}_{pt}\partial\boldsymbol{\theta}_{pt}^\top} = \begin{bmatrix} \frac{\partial^2\alpha_{pt}\mathbf{m}(\omega_{pt})}{\partial\Phi_{pt}^2} & \frac{\partial^2\alpha_{pt}\mathbf{m}(\omega_{pt})}{\partial\Phi_{pt}\partial\rho_{pt}} & \frac{\partial^2\alpha_{pt}\mathbf{m}(\omega_{pt})}{\partial\Phi_{pt}\partial\tau_{pt}} & \frac{\partial^2\mathbf{m}(\theta_{pt})}{\partial\Phi_{pt}\partial b_{pt}} \\ \frac{\partial^2\alpha_{pt}\mathbf{m}(\omega_{pt})}{\partial\rho_{pt}\partial\Phi_{pt}} & \frac{\partial^2\mathbf{m}(\theta_{pt})}{\partial\rho_{pt}^2} & \frac{\partial^2\alpha_{pt}\mathbf{m}(\omega_{pt})}{\partial\rho_{pt}\partial\tau_{pt}} & \frac{\partial^2\alpha_{pt}\mathbf{m}(\omega_{pt})}{\partial\rho_{pt}\partial b_{pt}} \\ \frac{\partial^2\alpha_{pt}\mathbf{m}(\omega_{pt})}{\partial\tau_{pt}\partial\Phi_{pt}} & \frac{\partial^2\alpha_{pt}\mathbf{m}(\omega_{pt})}{\partial\tau_{pt}\partial\rho_{pt}} & \frac{\partial^2\mathbf{m}(\theta_{pt})}{\partial\tau_{pt}^2} & \frac{\partial^2\alpha_{pt}\mathbf{m}(\omega_{pt})}{\partial\tau_{pt}\partial b_{pt}} \\ \frac{\partial^2\alpha_{pt}\mathbf{m}(\omega_{pt})}{\partial b_{pt}\partial\Phi_{pt}} & \frac{\partial^2\alpha_{pt}\mathbf{m}(\omega_{pt})}{\partial b_{pt}\partial\rho_{pt}} & \frac{\partial^2\mathbf{m}(\theta_{pt})}{\partial b_{pt}\partial\tau_{pt}} & \frac{\partial^2\alpha_{pt}\mathbf{m}(\omega_{pt})}{\partial b_{pt}^2} \end{bmatrix}, \tag{C.2}$$

$$\frac{\partial^2\alpha_{pt}\mathbf{m}(\omega_{pt})}{\partial\Phi_{pt}^2} = -\rho_{pt}e^{j\Phi_{pt}}s(t-\tau_{pt})e^{-j\omega_c b_{pt}(t-\tau_{pt})}, \tag{C.3}$$

$$\frac{\partial^2\alpha_{pt}\mathbf{m}(\omega_{pt})}{\partial\Phi_{pt}\partial\rho_{pt}} = je^{j\Phi_{pt}}s(t-\tau_{pt})e^{-j\omega_c b_{pt}(t-\tau_{pt})}, \tag{C.4}$$

$$\frac{\partial^2\alpha_{pt}\mathbf{m}(\omega_{pt})}{\partial\Phi_{pt}\partial\tau_{pt}} = -j\rho_{pt}e^{j\Phi_{pt}}s^{(1)}(t-\tau_{pt})e^{-j\omega_c b_{pt}(t-\tau_{pt})} - \omega_c b_{pt}\rho_{pt}e^{j\Phi_{pt}}s(t-\tau_{pt})e^{-j\omega_c b_{pt}(t-\tau_{pt})}, \tag{C.5}$$

$$\frac{\partial^2\alpha_{pt}\mathbf{m}(\omega_{pt})}{\partial\Phi_{pt}\partial b_{pt}} = \omega_c\rho_{pt}e^{j\Phi_{pt}}(t-\tau_{pt})s(t-\tau_{pt})e^{-j\omega_c b_{pt}(t-\tau_{pt})}, \tag{C.6}$$

$$\frac{\partial^2\alpha_{pt}\mathbf{m}(\omega_{pt})}{\partial\rho_{pt}\partial\Phi_{pt}} = je^{j\Phi_{pt}}s(t-\tau_{pt})e^{-j\omega_c b_{pt}(t-\tau_{pt})}, \tag{C.7}$$

$$\frac{\partial^2\alpha_{pt}\mathbf{m}(\omega_{pt})}{\partial\rho_{pt}^2} = 0, \tag{C.8}$$

$$\frac{\partial^2\alpha_{pt}\mathbf{m}(\omega_{pt})}{\partial\rho_{pt}\partial\tau_{pt}} = -e^{j\Phi_{pt}}s^{(1)}(t-\tau_{pt})e^{-j\omega_c b_{pt}(t-\tau_{pt})} + j\omega_c b_{pt}e^{j\Phi_{pt}}s(t-\tau_{pt})e^{-j\omega_c b_{pt}(t-\tau_{pt})}, \tag{C.9}$$

$$\frac{\partial^2\alpha_{pt}\mathbf{m}(\omega_{pt})}{\partial\rho_{pt}\partial b_{pt}} = -j\omega_c(t-\tau_{pt})e^{j\Phi_{pt}}s(t-\tau_{pt})e^{-j\omega_c b_{pt}(t-\tau_{pt})}, \tag{C.10}$$

$$\frac{\partial^2\alpha_{pt}\mathbf{m}(\omega_{pt})}{\partial\tau_{pt}\partial\Phi_{pt}} = -j\rho_{pt}e^{j\Phi_{pt}}s^{(1)}(t-\tau_{pt})e^{-j\omega_c b_{pt}(t-\tau_{pt})} - \omega_c b_{pt}\rho_{pt}e^{j\Phi_{pt}}s(t-\tau_{pt})e^{-j\omega_c b_{pt}(t-\tau_{pt})}, \tag{C.11}$$

$$\frac{\partial\alpha_{pt}\mathbf{m}(\omega_{pt})}{\partial\tau_{pt}\partial\rho_{pt}} = e^{j\Phi_{pt}}s^{(1)}(t-\tau_{pt})e^{-j\omega_c b_{pt}(t-\tau_{pt})} + j\omega_c b_{pt}e^{j\Phi_{pt}}s(t-\tau_{pt})e^{-j\omega_c b_{pt}(t-\tau_{pt})}, \tag{C.12}$$

$$\frac{\partial^2 \alpha_{pt}\mathbf{m}(\omega_{pt})}{\partial \tau_{pt}^2} = \rho_{pt} e^{j\Phi_{pt}} s^{(2)}(t-\tau_{pt}) e^{-j\omega_c b_{pt}(t-\tau_{pt})} - 2j\omega_c b_{pt}\rho_{pt} e^{j\Phi_{pt}} s^{(1)}(t-\tau_{pt}) e^{-j\omega_c b_{pt}(t-\tau_{pt})}$$

$$- \rho_{pt}\omega_c^2 b_{pt}^2 e^{j\Phi_{pt}} s(t-\tau_{pt}) e^{-j\omega_c b_{pt}(t-\tau_{pt})}, \tag{C.13}$$

$$\frac{\partial^2 \alpha_{pt}\mathbf{m}(\omega_{pt})}{\partial \tau_{pt}\partial b_{pt}} = j\omega_c \rho_{pt} e^{j\Phi_{pt}} (t-\tau_{pt}) s^{(1)}(t-\tau_{pt}) e^{-j\omega_c b_{pt}(t-\tau_{pt})} + j\omega_c \rho_{pt} e^{j\Phi_{pt}} s(t-\tau_{pt}) e^{-j\omega_c b_{pt}(t-\tau_{pt})}$$

$$+ \rho_{pt}\omega_c^2 b_{pt} e^{j\Phi_{pt}} (t-\tau_{pt}) s(t-\tau_{pt}) e^{-j\omega_c b_{pt}(t-\tau_{pt})}, \tag{C.14}$$

$$\frac{\partial^2 \alpha_{pt}\mathbf{m}(\omega_{pt})}{\partial b_{pt}\partial \Phi_{pt}} = \omega_c \rho_{pt} e^{j\Phi_{pt}} (t-\tau_{pt}) s(t-\tau_{pt}) e^{-j\omega_c b_{pt}(t-\tau_{pt})}, \tag{C.15}$$

$$\frac{\partial^2 \alpha_{pt}\mathbf{m}(\omega_{pt})}{\partial b_{pt}\partial \rho_{pt}} = -j\omega_c b_{pt} e^{j\Phi_{pt}} (t-\tau_{pt}) s(t-\tau_{pt}) e^{-j\omega_c b_{pt}(t-\tau_{pt})}, \tag{C.16}$$

$$\frac{\partial^2 \alpha_{pt}\mathbf{m}(\omega_{pt})}{\partial b_{pt}\partial \tau_{pt}} = j\omega_c \rho_{pt} e^{j\Phi_{pt}} (t-\tau_{pt}) s^{(1)}(t-\tau_{pt}) e^{-j\omega_c b_{pt}(t-\tau_{pt})} + j\omega_c \rho_{pt} e^{j\Phi_{pt}} s(t-\tau_{pt}) e^{-j\omega_c b_{pt}(t-\tau_{pt})}$$

$$+ \rho_{pt}\omega_c^2 b_{pt} e^{j\Phi_{pt}} (t-\tau_{pt}) s(t-\tau_{pt}) e^{-j\omega_c b_{pt}(t-\tau_{pt})}, \tag{C.17}$$

$$\frac{\partial^2 \alpha_{pt}\mathbf{m}(\omega_{pt})}{\partial b_{pt}^2} = -\rho_{pt}\omega_c^2 e^{j\Phi_{pt}} (t-\tau_{pt})^2 s(t-\tau_{pt}) e^{-j\omega_c b_{pt}(t-\tau_{pt})}. \tag{C.18}$$

Note that we can express (C.2) as a product of the exponential terms and a matrix product,

$$\frac{\partial^2 \alpha_{pt}\mathbf{m}(\omega_{pt})}{\partial \boldsymbol{\theta}_{pt}\partial \boldsymbol{\theta}_{pt}^\top} = e^{j\Phi_{pt}} e^{-j\omega_c b_{pt}(t-\tau_{pt})} \mathbf{Q}_T \left(\boldsymbol{\vartheta} \otimes \mathbf{I}_4\right), \tag{C.19}$$

with $\otimes$ the Kronecker product, and $\mathbf{Q}_T = \begin{bmatrix}\mathbf{Q}_1 & \mathbf{Q}_2 & \mathbf{Q}_3 & \mathbf{Q}_4 & \mathbf{Q}_5 & \mathbf{Q}_6\end{bmatrix}$. Each matrix $\mathbf{Q}_i$ is multiplied by the i^{th} element of the signal sample vector,

$$\boldsymbol{\vartheta} = \begin{bmatrix} s(t-\tau_{pt}) \\ (t-\tau_{pt})s(t-\tau_{pt}) \\ s^{(1)}(t-\tau_{pt}) \\ (t-\tau_{pt})s^{(1)}(t-\tau_{pt}) \\ s^{(2)}(t-\tau_{pt}) \\ (t-\tau_{pt})^2 s(t-\tau_{pt}) \end{bmatrix}, \tag{C.20}$$

$$\mathbf{Q}_1 = \begin{bmatrix} -\rho_{pt} & j & -\omega_c b_{pt}\rho_{pt} & 0 \\ j & 0 & j\omega_c b_{pt} & 0 \\ -\omega_c b_{pt}\rho_{pt} & j\omega_c b_{pt} & -\rho_{pt}\omega_c^2 b_{pt}^2 & j\omega_c\rho_{pt} \\ 0 & 0 & j\omega_c\rho_{pt} & 0 \end{bmatrix}, \ \mathbf{Q}_2 = \begin{bmatrix} 0 & 0 & 0 & \omega_c\rho_{pt} \\ 0 & 0 & 0 & -j\omega_c \\ 0 & 0 & 0 & \rho_{pt}\omega_c^2 b_{pt} \\ \omega_c\rho_{pt} & -j\omega_c b_{pt} & \rho_{pt}\omega^2 b_{pt} & 0 \end{bmatrix},$$

$$\mathbf{Q}_3 = \begin{bmatrix} 0 & 0 & -j\rho_{pt} & 0 \\ 0 & 0 & -1 & 0 \\ -j\rho_{pt} & -1 & -2j\omega_c b_{pt}\rho_{pt} & 0 \\ 0 & 0 & 0 & 0 \end{bmatrix}, \ \mathbf{Q}_4 = \begin{bmatrix} 0 & 0 & 0 & 0 \\ 0 & 0 & 0 & 0 \\ 0 & 0 & 0 & j\omega_c\rho_{pt} \\ 0 & 0 & j\omega_c\rho_{pt} & 0 \end{bmatrix},$$

$$\mathbf{Q}_5 = \begin{bmatrix} 0 & 0 & 0 & 0 \\ 0 & 0 & 0 & 0 \\ 0 & 0 & \rho_{pt} & 0 \\ 0 & 0 & 0 & 0 \end{bmatrix}, \ \mathbf{Q}_6 = \begin{bmatrix} 0 & 0 & 0 & 0 \\ 0 & 0 & 0 & 0 \\ 0 & 0 & 0 & 0 \\ 0 & 0 & 0 & -\rho_{pt}\omega_c^2 \end{bmatrix}.$$

Finally, we write the product in a shorter form for concise equations,

$$\mathbf{M} = \mathbf{Q}_T \left(\boldsymbol{\vartheta} \otimes \mathbf{I}_4\right). \tag{C.21}$$

The steps to get a presentable form of the MCRB matrix are not trivial but consist of large and tedious matrix equations. The goal of this Appendix is to provide a closed-form for (20) by substituting and simplifying the result of (C.1). For the sake of shorthand notations and highlighting the key terms to simplify, we note the second derivative as $\frac{\partial^2 \alpha_{pt}\mathbf{m}(\omega_{pt})}{\partial \boldsymbol{\theta}_{pt} \partial \boldsymbol{\theta}_{pt}^\top} = e^{j\Phi_{pt}} e^{-j\omega_c b_{pt}(t-\tau_{pt})}\mathbf{M}$, where $\mathbf{M}$ is the matrix from (C.21). The product between this simplified form and (24) can be easily simplified,

$$(\delta \mathbf{m})^H \left(\frac{\partial^2 \alpha_{pt}\mathbf{m}(\boldsymbol{\omega}_{pt})}{\partial \boldsymbol{\theta}_{pt} \partial \boldsymbol{\theta}_{pt}^\top}\right) = \rho_{pt} s^H(t-\tau_{pt}) \left(e^{\Psi(t)}\mathbf{M} - \mathbf{M}\right). \tag{C.22}$$

With this simpler form, we can compute $\mathbf{A}(\boldsymbol{\theta}_{pt})$ as,

$$\begin{aligned} \mathbf{A}(\boldsymbol{\theta}_{pt}) &= \tfrac{2f_s\rho_{pt}}{\sigma_n^2}\mathrm{Re}\left\{e^{\Psi(t)}s^H(t-\tau_{pt})\mathbf{M} - s^H(t-\tau_{pt})\mathbf{M}\right\} - \tfrac{2f_s\rho_{pt}}{\sigma_n^2}\mathrm{Re}\left\{\boldsymbol{Q}\boldsymbol{W}\boldsymbol{Q}^H\right\} \\ &= \tfrac{2f_s\rho_{pt}}{\sigma_n^2}\mathrm{Re}\left\{e^{\Psi(t)}s^H(t-\tau_{pt})\mathbf{M}\right\} - \tfrac{2f_s\rho_{pt}}{\sigma_n^2}\mathrm{Re}\left\{s^H(t-\tau_{pt})\mathbf{M} + \boldsymbol{Q}\boldsymbol{W}\boldsymbol{Q}^H\right\} \\ &= \tfrac{2f_s\rho_{pt}}{\sigma_n^2}\mathrm{Re}\left\{e^{\Psi(t)}s^H(t-\tau_{pt})\mathbf{M}\right\} - \tfrac{2f_s\rho_{pt}}{\sigma_n^2}\begin{bmatrix} 0 & 0 & 0 & 0 \\ 0 & \frac{w_1}{\rho_{pt}} & 0 & 0 \\ 0 & 0 & 0 & 0 \\ 0 & 0 & 0 & 0 \end{bmatrix} = \tfrac{2f_s\rho_{pt}}{\sigma_n^2}\mathrm{Re}\left\{\boldsymbol{\chi}\right\} \end{aligned} \tag{C.23}$$

where $\mathrm{Re}\left\{s^H(t-\tau_{pt})\mathbf{M}\right\}$ is given in (C.24) with w_M defined in the following Appendix D. To obtain a closed-form expression of $\mathbf{A}(\boldsymbol{\theta}_{pt})$, the final step is to derive a closed-form of the new integrals that arise from the definition in (27).

$$\begin{bmatrix} -w_1\rho & 0 & -\rho w_c b w_1 + \rho \mathrm{Im}\{w_3\} & \rho w_c w_2 \\ 0 & 0 & -\mathrm{Re}\{w_3\} & 0 \\ -\rho w_c b w_1 + \rho\mathrm{Im}\{w_3\} & -\mathrm{Re}\{w_3\} & -w_c^2\rho b^2 w_1 + \rho w_M + 2w_c\rho b \cdot \mathrm{Im}\{w_3\} & w_c^2\rho b w_2 - \rho w_c \mathrm{Im}\{W_{3,2}\} \\ \rho w_c w_2 & 0 & w_c^2 \rho b w_2 - \rho w_c\mathrm{Im}\{W_{3,2}\} & -\rho w_c^2 W_{2,2} \end{bmatrix}. \tag{C.24}$$

Appendix D. Derivation of the χ Coefficients

The first new term to be derived is w_M. It requires the definition of the second derivative of the signal $s(t)$, which is expressed as $s^{(2)}(t)$. We use a property of Fourier transforms to convert the integral to the frequency domain: $s(t) \rightleftharpoons S(f)$ and $s^{(2)}(t) \rightleftharpoons -4\pi^2 f^2 S(f)$. Moreover, $S(f) = \frac{1}{f_s}\sum_{k=N_1}^{N_2} s(kT_s)e^{-j2\pi\frac{f}{f_s}k}$ and $S^{(1)}(f) = \frac{-j2\pi}{f_s^2}\sum_{k=N_1}^{N_2} ks(kT_s)e^{-j2\pi\frac{f}{f_s}k}$. Then,

$$
\begin{aligned}
w_M &= \int_{-\infty}^{\infty} s^*(t-\tau)s^{(2)}(t-\tau)dt \rightleftharpoons \int_{-\frac{f_s}{2}}^{\frac{f_s}{2}} -4\pi^2 f^2 (S(f))^* S(f) df \\
&= -f_s \int_{-\frac{1}{2}}^{\frac{1}{2}} 4\pi^2 f^2 |S(f)|^2 df - f_s \int_{-\frac{1}{2}}^{\frac{1}{2}} 4\pi^2 f^2 |\boldsymbol{v}^H(f)\mathbf{s}|^2 = -f_s \mathbf{s}^H \mathbf{V}\mathbf{s} = -W_{3,3},
\end{aligned} \tag{D.1}
$$

with $\boldsymbol{v}(f) = \left(e^{j2\pi f N_1}, \cdots, e^{j2\pi f 0, \cdots, e^{j2\pi f N_2}}\right)^T$ and $\mathbf{V} = 4\pi^2 \int_{-\frac{1}{2}}^{\frac{1}{2}} f\boldsymbol{v}(f)\boldsymbol{v}(f)^H$ with closed-form defined in (B.6). To compute a closed-form of $\mathrm{Re}\{\chi\}$, the integral terms in (28) can be computed in terms of the existing integrals defined in [10],

$$
\begin{aligned}
w_{e_1} &= \int_{-\infty}^{\infty} s^*(t-\tau)s(t-\tau)e^{-j\omega_c d(T_e(t-\tau)-(t-\tau)^2)}dt \\
&= \int_{-\infty}^{\infty} s^*(t-\tau)s(t-\tau)[1-j\omega_c dT_e(t-\tau)]dt = w_1 - j\omega_c dT_e w_2,
\end{aligned}
$$

where the exponential term has been approximated as $e^{-j\omega_c d\left(T_e(t-\tau)-(t-\tau)^2\right)} \approx 1 - j\omega_c dT_e(t-\tau)$. We emphasize that this approximation is valid since the product $d \cdot Te$ and the value $t-\tau$ are small. Making the same approximation to derive the remaining terms,

$$
\begin{aligned}
w_{e_2} &= \int_{-\infty}^{\infty} (t-\tau)s^*(t-\tau)s(t-\tau)e^{-j\omega_c d(T_e(t-\tau)-(t-\tau)^2)}dt \\
&= \int_{-\infty}^{\infty} (t-\tau)s^*(t-\tau)s(t-\tau)[1-j\omega_c dT_e(t-\tau)]dt = w_2 - j\omega_c dT_e W_{2,2},
\end{aligned}
$$

$$
\begin{aligned}
w_{e_3} &= \int_{-\infty}^{\infty} s^*(t-\tau)s^{(1)}(t-\tau)e^{-j\omega_c d(T_e(t-\tau)-(t-\tau)^2)}dt = \int_{-\infty}^{\infty} s^*(t-\tau)s^{(1)}(t-\tau)[1-j\omega_c dT_e(t-\tau)]dt \\
&= w_3 - j\omega_c dT_e W_{3,2},
\end{aligned}
$$

$$
\begin{aligned}
W_{e_{3,2}} &= \int_{-\infty}^{\infty} (t-\tau)s^*(t-\tau)s^{(1)}(t-\tau)e^{-j\omega_c d(T_e(t-\tau)-(t-\tau)^2)}dt \\
&= \int_{-\infty}^{\infty} (t-\tau)s^*(t-\tau)s^{(1)}(t-\tau)[1-j\omega_c dT_e(t-\tau)]dt = W_{3,2} - j\omega_c dT_e W_{4,3},
\end{aligned}
$$

with $W_{4,3} = \frac{1}{f_s^2}\left(\mathbf{s}^H\mathbf{D}\boldsymbol{\Lambda}\mathbf{D}\mathbf{s} - \mathbf{s}^H\mathbf{D}\mathbf{s}\right)$, following the notation used in [11], and derived for first time in [25].

$$
\begin{aligned}
W_{e_{2,2}} &= \int_{-\infty}^{\infty} (t-\tau)^2 s^*(t-\tau)s(t-\tau)e^{-j\omega_c d(T_e(t-\tau)-(t-\tau)^2)}dt \\
&= \int_{-\infty}^{\infty} (t-\tau)^2 s^*(t-\tau)s(t-\tau)[1-j\omega_c dT_e(t-\tau)]dt = W_{2,2} - j\omega_c dT_e W_{4,2},
\end{aligned}
$$

with $W_{4,2} = \frac{1}{f_s^4}\left(\mathbf{s}^H\mathbf{D}^3\mathbf{s}\right)$ derived in [11].

$$
\begin{aligned}
w_{e_M} &= \int_{-\infty}^{\infty} s^*(t-\tau)s^{(2)}(t-\tau)e^{-j\omega_c d(T_e(t-\tau)-(t-\tau)^2)}dt \\
&= \int_{-\infty}^{\infty} s^*(t-\tau)s^{(2)}(t-\tau)[1-j\omega_c dT_e(t-\tau)+]dt = -W_{3,3} - j\omega_c dT_e w_{M,2},
\end{aligned}
$$

with $w_{M,2}$ computed using the same property of the Fourier transform from (D.1),

$$\begin{aligned} w_{M,2} &= \int_{-\infty}^{\infty} (t-\tau) s^*(t-\tau) s^{(2)}(t-\tau) dt \rightleftharpoons \int_{-\frac{f_s}{2}}^{\frac{f_s}{2}} \left(\frac{j}{2\pi} S^{(1)}(f)\right)^* \left(-4\pi^2 f^2 S(f)\right) df \\ &= -\int_{-\frac{1}{2}}^{\frac{1}{2}} (\mathbf{D}\mathbf{s})^H \boldsymbol{\nu}(f) \left(4\pi^2 f^2 \mathbf{s} \boldsymbol{\nu}^H(f)\right) df = -\mathbf{s}^H \mathbf{D}\mathbf{V}\mathbf{s}. \end{aligned} \tag{D.2}$$

This marks the last integral term needed to compute the closed-form MCRB for joint delay and Doppler estimation. For the acceleration parameter $d = 0$, the integral equations simplify to the existing CRB equations for joint delay and Doppler estimation.

References

[1] P. J. G. Teunissen, O. Montenbruck (Eds.), Handbook of Global Navigation Satellite Systems, Springer, Switzerland, 2017.

[2] H. L. Van Trees, Detection, estimation, and modulation theory, Part III: Radar – Sonar Signal Processing and Gaussian Signals in Noise, John Wiley & Sons, 2001.

[3] L. L. Scharf, Statistical signal processing: detection, estimation, and time series analysis, Addison-Wesley, 2002.

[4] H. L. Van Trees, Optimum Array Processing, Wiley-Interscience, New-York, 2002.

[5] P. J. Schreier, L. L. Scharf, Statistical Signal Processing of Complex-Valued Data, Cambridge University Press, 2010.

[6] C. D. Richmond, L. L. Horowitz, Parameter bounds on estimation accuracy under model misspecification, IEEE Transactions on Signal Processing 63 (9) (2015) 2263–2278. doi:10.1109/TSP.2015.2411222.

[7] M. L. Diong, E. Chaumette, F. Vincent, On the efficiency of maximum-likelihood estimators of misspecified models, in: 25th European Signal Processing Conference (EUSIPCO), 2017, pp. 1455–1459.

[8] Z. Ben-Haim, Y. C. Eldar, The Cramér-Rao bound for estimating a sparse parameter vector, IEEE Transactions on Signal Processing 58 (6) (2010) 3384–3389. doi:10.1109/TSP.2010.2045423.

[9] R. Prasad, C. R. Murthy, Cramér-Rao-type bounds for sparse bayesian learning, IEEE Transactions on Signal Processing 61 (3) (2013) 622–632. doi:10.1109/tsp.2012.2226165.
URL https://doi.org/10.1109%2Ftsp.2012.2226165

[10] D. Medina, L. Ortega, J. Vilà-Valls, P. Closas, F. Vincent, E. Chaumette, A New Compact CRB for Delay, Doppler and Phase Estimation-Application to GNSS SPP & RTK Performance Characterization, IET Radar Sonar & Navigation 14 (2020) 1537–1549.

[11] H. McPhee, L. Ortega, J. Vilà-Valls, E. Chaumette, On the accuracy limit of joint time-delay/doppler/acceleration estimation with a band-limited signal, in: ICASSP 2021 - 2021 IEEE International Conference on Acoustics, Speech and Signal Processing (ICASSP), 2021, pp. 5130–5134. doi:10.1109/ICASSP39728.2021.9414270.

[12] A. Renaux, P. Forster, E. Chaumette, P. Larzabal, On the high-SNR conditional maximum-likelihood estimator full statistical characterization, IEEE Trans. on SP 54 (12) (2006) 4840 – 4843.

[13] S. Fortunati, F. Gini, M. S. Greco, C. D. Richmond, Performance bounds for parameter estimation under misspecified models: Fundamental findings and applications, IEEE Signal Processing Magazine 34 (6) (2017) 142–157.

[14] A. Mennad, S. Fortunati, M. N. El Korso, A. Younsi, A. M. Zoubir, A. Renaux, Slepian-Bangs-type formulas and the related Misspecified Cramér-Rao Bounds for Complex Elliptically Symmetric distributions, Signal Processing 142 (2018) 320–329. doi:10.1016/j.sigpro.2017.07.029.
URL https://hal.parisnanterre.fr//hal-01654607

[15] Q. H. Vuong, Cramér-Rao bounds for misspecified models, working paper 652, Div. of the Humanities and Social Sci., Caltech, Pasadena, USA, 1986.

[16] S. Fortunati, F. Gini, M. S. Greco, The misspecified Cramér-Rao bound and its application to scatter matrix estimation in complex elliptically symmetric distributions, IEEE Transactions on Signal Processing 64 (9) (2016) 2387–2399.

[17] P. J. Huber, The behavior of maximum likelihood estimates under nonstandard conditions,, in: in Proceedings of the Fifth Berkeley Symposium in Mathematical Statistics and Probability, 1967, pp. 1–6.

[18] H. White, Maximum likelihood estimation of misspecified models, Econometrica: Journal of the econometric society (1982) 1–25.

[19] S. J. Orfanidis, Electromagnetic Waves and Antennas, Rutgers University, 2016.
URL `www.ece.rutgers.edu/~orfanidi/ewa`

[20] M. I. Skolnik, Radar Handbook, 3rd Edition, McGraw-Hill, New York, USA, 1990.

[21] E. J. Kelly, The Radar Measurement of Range, Velocity and Acceleration, IRE Transactions on Military Electronics (1961) 51–57.

[22] H. Akaike, Information Theory and an Extension of the Maximum Likelihood Principle,, in: in Proceeding of IEEE ISIT,, 1973.

[23] B. Ottersten, M. Viberg, P. Stoica, A. Nehorai, Exact and large sample maximum likelihood techniques for parameter estimation and detection in array processing, in: S. Haykin, J. Litva, T. J. Shepherd (Eds.), Radar Array Processing, Springer-Verlag, Heidelberg, 1993, Ch. 4, pp. 99–151.

[24] Q. Ding, S. Kay, Maximum likelihood estimator under a misspecified model with high signal-to-noise ratio, IEEE Transactions on Signal Processing 59 (8) (2011) 4012–4016. `doi:10.1109/TSP.2011.2150220`.

[25] P. Das, J. Vilà-Valls, F. Vincent, L. Davain, E. Chaumette, A new compact delay, doppler stretch and phase estimation crb with a band-limited signal for generic remote sensing applications., Remote Sensing 12 (2) (2020) 2913.

[26] B. Badke, What is c/n0 and how is it calculated in a gnss receiver ?, Inside GNSS (2009) 20–23.

[27] S. Walker, Atmospheric descent (https://www.mathworks.com/matlabcentral/fileexchange/26121-atmospheric-descent), matlab central file exchange, retrieved December 6, 2021.

[28] L. Ortega, J. Vilà-Valls, E. Chaumette, F. Vincent, On the Time-Delay Estimation Performance Limit of New GNSS Acquisition Codes, in: ICL-GNSS 2020, IEEE, 2020, pp. 1–6.